Gemstones: A Model Suite for Multi-Faceted Scaling Laws

Sean McLeish^{1*}, John Kirchenbauer¹, David Yu Miller¹, Siddharth Singh¹
Abhinav Bhatele¹, Micah Goldblum², Ashwinee Panda¹, Tom Goldstein¹

1 University of Maryland, ² Columbia University

Abstract

Scaling laws are typically fit using a family of models with a narrow range of frozen hyper-parameter choices. In this work we study scaling laws using multiple architectural shapes and hyperparameter choices, highlighting their impact on resulting prescriptions. As a primary artifact of our research, we release the *Gemstones*: an open-source scaling law dataset, consisting of over 4000 checkpoints from transformers with up to 2 billion parameters and diverse architectural shapes; including ablations over learning rate and cooldown. Our checkpoints enable more complex studies of scaling, such as analyzing the relationship between width and depth. By examining our model suite, we find that the prescriptions of scaling laws can be highly sensitive to the experimental design process and the specific model checkpoints used during fitting.

Code: github.com/mcleish7/gemstone-scaling-laws

1 Introduction

Existing works on scaling laws often restrict Transformer architectures to a small range of width-depth ratios [Porian et al., 2024], train on a small number of tokens, and fix training hyperparameters such as cooldown schedule across training runs [Hoffmann et al., 2022]. These design choices, in turn, can dramatically influence the resulting scaling laws. If a scaling law is sensitive to such design choices, then it may only be useful for practitioners implementing similar setups to those that produced the scaling law. In practice, practitioners often take guidance from scaling laws that assume completely different design choices than their own implementation, often without understanding to degree to which these choices may impact optimal scaling.

In this work, we produce a vast array of model checkpoints for studying how model design and model selection impact scaling laws. Our models, called the *Gemstones* because they are loosely based on scaled-down variants of the Gemma architecture, vary in their parameter count, width/depth ratio, training tokens, learning rates, and cooldown schedules. By fitting scaling laws to these checkpoints, we confirm that scaling law parameters and interpretations indeed depend strongly on the selection of models and fitting procedure used, and we quantify the degree to which these decisions impact predictions. By exploiting the variation among our model checkpoints, we also analyze the impact

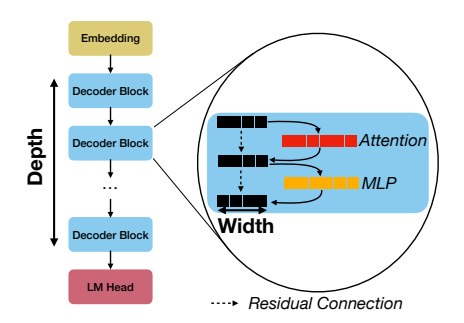


Figure 1: **The meaning of width and depth.** We visualize a standard transformer architecture, highlighting the "width" as the size of the hidden dimension and the "depth" as the number of transformer blocks.

^{*}Correspondence to: smcleish@umd.edu.

of architectural shape across loss, benchmark performance and training time with findings consistent with design choices we see in industry models. Our contributions are summarized as follows:

We open-source more than 4000 checkpoints cumulatively trained on over 10 trillion tokens. The models we provide are diverse across architectural and training hyperparameter axes, enabling more granular studies than previous work (see Figure 2).

We highlight the fragility and common pitfalls of prior scaling laws. There are many decisions to make when choosing points to fit scaling laws that significantly change the slope of the law (see Table 1).

We analyze the impact of model shape on loss, benchmarks and training time. We find that although deep models achieve lower loss and benchmark error when measured using floating point operations, they require significantly more training time when using typical open-source parallelism frameworks (see Figures 4, 7 and 8).

2 Related Work

Scaling laws address the trade-off between parameter count and number of training tokens, attempting to find the minimum loss possible for a language model with a constrained floating point operation (FLOP) budget. The body of work on scaling laws is vast. Therefore, while we provide a brief overview of key prior work here to contextualize our contributions, we also include an extended literature review in Section B.

Design Choices for Scaling Laws Scaling laws often treat model design and training as if it has a single dimension (parameter count), while, in practice, training is sensitive to many choices. Notably, Hoffmann et al. [2022] find significantly different fitted laws (Equation (1)) compared to Kaplan et al. [2020]. Pearce and Song [2024] and Porian et al. [2024] attribute most of this discrepancy to the choice to exclude embedding parameters from the parameter count, both showing one law can be transformed into the other via controlled changes. Kaplan et al. [2020] justify excluding embedding parameters by showing that non-embedding parameters have a cleaner relationship with test loss. Scaling laws are also commonly included in many large model releases [Hu et al., 2024, Bi et al., 2024, Dubey et al., 2024].

Choshen et al. [2024] collect both loss and benchmark performance metrics for a multitude of models and offer a practitioner's guide to fitting scaling laws. Notably, they suggest that 5 models are ample to fit a scaling law, and that you should omit the early part of training when fitting, because those early steps don't follow the same scaling behavior and can skew the results. In contrast, Li et al. [2024c] demonstrate that varying the tokens-per-parameter ratio and relying on limited grid searches when fitting scaling laws can lead to large variations in results. Hägele et al. [2024] suggest that a constant learning rate plus cooldown is preferable to a cosine learning rate schedule as all intermediate checkpoints can be used for fitting. The authors also find that stochastic weight averaging should be encouraged in scaling law analysis as it tends to lead to better models. Furthermore, Inbar and Sernau [2024] observe that FLOPs cannot be used to predict wall-clock time nor memory movement, and suggest that fast-training architectures may be preferred over those prescribed by scaling laws.

There are multiple works analyzing whether scaling laws can be used to predict downstream performance. Bhagia et al. [2024] first predict task-specific loss and then use this to predict performance on the task, using a sigmoidal function to map from loss to accuracy. Gadre et al. [2024] predict top-1 error, fitting a power law function on the perplexity of the model to predict error. Gadre et al. [2024] also look at the impact of overtraining, finding scaling laws that extrapolate with the amount of overtraining. Dey et al. [2023] analyze the trade off of inference FLOPs and training FLOPs using scaling laws to prescribe training configurations that balance training and inference. Unfortunately, both Dey et al. [2023] and Biderman et al. [2023] train on the Pile [Gao et al., 2020] which has since been taken down due to copyright, leaving a gap for a model collection in the open literature.

The Role of Model Shape Another line of research specifically studies the interplay between model width and model depth; for clarity we visualize our working definitions for these dimensions in Figure 1. Levine et al. [2020] find that, for large models, optimal depth grows logarithmically with width. Henighan et al. [2020] find there is an optimal aspect ratio for each modality they study which

gives maximum performance: for example, they find 5 to be optimal for math models. Team et al. [2024b] compare two 9 billion parameter models and find the deeper model outperforms the wider one consistently across benchmarks. Unfortunately, the authors are vague about the specific details of this result. Petty et al. [2024] claim small (<400M) transformers have diminishing benefits from depth. Brown et al. [2022] show that in some cases shallower models can beat their parameter-equivalent deep models on tasks for encoder-decoder transformer architectures. These results differ from Kaplan et al. [2020] who suggest aspect ratio is not a determining factor for final loss. Tay et al. [2022] show that downstream performance strongly depends on shape when finetuning but pretraining perplexity does not. Alabdulmohsin et al. [2024] study the impact of width and depth for encoder-decoder vision transformers, using their laws to create a smaller transformer model which has competitive downstream performance when compared with much larger models. The architecture found in this study has since been used by Beyer et al. [2024] in PaliGemma. Concurrently, Zuo et al. [2025] study the impact of width and depth in hybrid architectures, finding that a deeper 1.5B model can match or even outperform 3B and 7B models.

As discussed above, the literature on how the aspect ratio of a LLM affects its performance and scaling characteristics is simultaneously extensive but somewhat inconclusive. While we do not presume to fully answer every question in this space, the experiments we describe in the rest of this work make progress on how to understand the results of prior studies and the impacts of certain architecture choices in a fully open, reproducible, and extensible way.

3 Designing Our Scaling Laws

We discuss the design of our scaling laws, including model selection, the choice of learning rate, and curve fitting schemes in the subsequent sections and in greater detail in Section A.

Architecture. To reduce the search space of all possible models, we add some constraints, each of which are either based on precedent from a popular model series like Gemma [Team et al., 2024a,b], Llama [Touvron et al., 2023], Pythia [Biderman et al., 2023], or practical considerations such as hardware details (see Section A).

Within these constraints, we search the set of feasible models within target parameter count groups 50M, 100M, 500M, 1B and 2B with a tolerance of $\pm 5\%$. At smaller scales we train up to 5 models at diverse widths and depths. At large parameter counts we train only 3 models, aiming for one "standard" aspect ratio (similar to existing models), one "wide" model, and one "deep" model. We visualize the models we choose to train in Figure 2 overlaid with a selection of existing models from prior work. In the Appendix, we plot the entire discrete set of all possible models under our constraints (Figure 10). Our 22 different models range from 50M to 2B parameters, spanning 11 widths from 256 to 3072 and 18 depths from 3 to 80.

Polishing the Gemstones. For the main set of training runs, we train each model for 350B tokens of Dolma 1.7 [Soldaini et al., 2024] data. We target a total batch size of 4 million tokens following[Touvron et al., 2023, Dubey et al., 2024, Bai et al., 2023], with a context length of

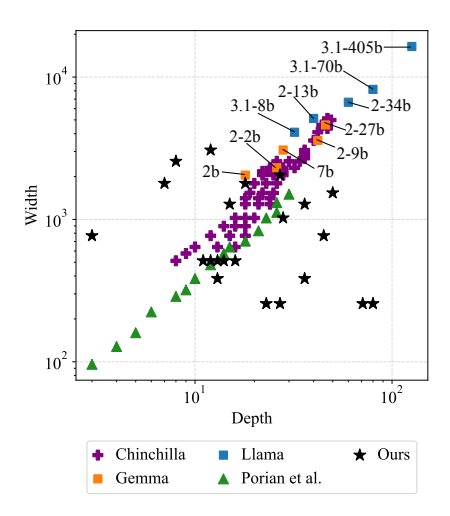


Figure 2: **Distribution of prior scaling law models, industry models, and our models in terms of width and depth.** Prior work (purple and green) and industry models (blue and orange) mostly lie on a fixed width-depth line.

2048 and a world batch size of 2048 sequences. Following Hägele et al. [2024] and Hu et al. [2024], we use a linear learning rate warm up over 80 million tokens, and then train at a constant learning rate, which we adjust for model size as described in Section A.1.

In service of future research based on our model suite, we open source checkpoints for all models at 2 billion token intervals, amounting to over 4,000 checkpoints in total. We also open source the fitting code and logged metrics for all runs.

We perform ablations over both cooldown and learning rate. For the cooldown ablation, we take the checkpoints saved every 10 billion tokens for the the first 100 billion tokens of training and cool these down, creating a second set of models which have had their learning rate annealed to 0 linearly. Specifically, we cool each model down by training for a further 10% of the total tokens which it has seen during training, i.e. our cooled down set of models have training budgets ranging from 11 to 110 billion tokens. We also ablate our choice of learning rate by running all models for 100 billion tokens with half of the learning rate we use for our main analysis. The full details of the scalable learning rate and parameter initialization scheme—designed to enable hyperparameter transfer across model sizes and aspect ratios—are provided in Section A.1.

Training Details We train with AdamW [Loshchilov and Hutter, 2017] with β parameters 0.9 and 0.95 and a weight decay of 0.1. We do not apply weight decay to the bias or normalization parameters. All models are trained with tensor parallelism [Singh and Bhatele, 2022, Singh et al., 2024] over multiple nodes of AMD MI250X GPUs. To the best of our knowledge, this makes the Gemstone suite of models the largest collection trained on AMD GPUs.

3.1 Fitting Scaling Laws

We fit scaling laws using methods similar to approach 1 and 3 from Chinchilla [Hoffmann et al., 2022]. We fit all laws using the log perplexity of all trained models on a sample of 100 million tokens from a fixed, held-out validation set from the training distribution. We also collect log perplexity values for a range of open source models [Team et al., 2024a,b, Touvron et al., 2023, Dubey et al., 2024, Yang et al., 2024a,b] on the same validation data to allow for a comparison between our predictions and a selection of widely used models. We design a specialized FLOP counting function as we find that simple rules of thumb (e.g., FLOPs per token= $6 \times parameters$ [Hoffmann et al., 2022]) do not accurately account for differences in FLOPs between extremely wide and narrow architectures. We discuss this further and present our function in Section L.

Following Porian et al. [2024], we plot the Epoch AI Replication [Besiroglu et al., 2024] of Chinchilla [Hoffmann et al., 2022] on all plots and use the coefficients for Kaplan plotted by Porian et al. [2024] which were extracted from the original paper [Kaplan et al., 2020].

A More Robust Approach to Fitting Compute-Optimal Laws. The first approach in Hoffmann et al. [2022] fits a scaling law by plotting the loss against FLOPs for a family of models with a range of parameter counts (but relatively consistent aspect ratio, see Figure 2) while varying dataset size, then fitting a line to the pareto-optimal architecture for each FLOP count (see Figure 3). Following Hoffmann et al. [2022], we refer to this as "Approach 1". As we use a constant learning rate, we can use all recorded validation losses to fit our law. Hoffmann et al. [2022] and Kaplan et al. [2020] select model shapes so densely that they have a near-optimal architecture at each FLOP count. This works when all architectures lie in a 1D space (parameterized by parameter count), as each model is optimal in some FLOP regime, and the lower envelope is densely populated. However, in our two dimensional exploration (varying width and depth), some models are never optimal, and the ones that are do not densely populate the envelope. We therefore develop a novel fitting method to accommodate sampling strategies like ours that result in regions of lower data density.

Our New Method: The Convex Hull. We fit a lower *convex hull* to our loss curves. This hull is only supported by a sparse set of optimal models. Fitting on only the vertices of this hull naturally excludes sub-optimal models that lie above the convex hull of optimality, and as we show in Section 4, this makes the resulting scaling law far more robust to model selection choices.

Why We Skip Approach 2. Another method to fit scaling laws is to put model runs into isoFLOP bins and choose the best parameter count in each bin. Hoffmann et al. [2022] call this "Approach 2". Our 2-dimensional set of models do not finely cluster into isoFLOP bins, meaning our data is not easily amenable to Approach 2, hence we exclude this approach from our analysis. Hu et al. [2024] and Li et al. [2024c] also eschew this approach.

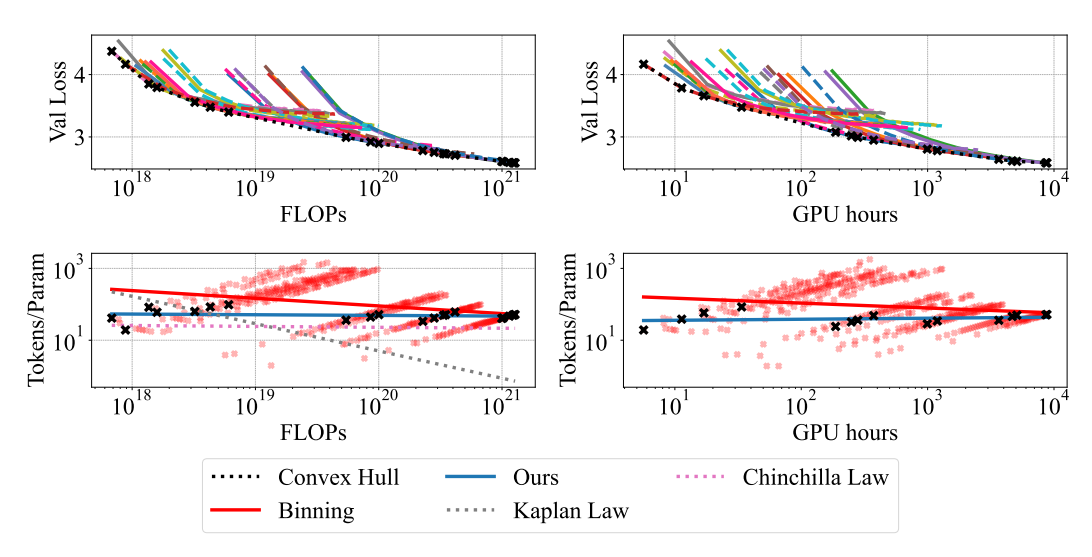


Figure 3: **Approach 1 prescriptions.** Row one: Validation loss over FLOPs (left) and GPU hours (right) for the first 100 billion tokens of training. We use Approach 1 to find the optimal points on the convex hull in each setting, marked with **black crosses**. Row two: We fit a line to the tokens per parameter of empirically optimal models and find a slightly higher, but still constant, tokens per parameter prescription than Hoffmann et al. [2022]. Hoffmann et al. [2022]'s Approach 1 creates 250 logarithmically-spaced FLOPs bins per order of magnitude, and in **red** we plot the minimizers over these bins, and the scaling law fitted to these minimizers (binning). Clearly, their Approach 1 is not well-suited for our data, and our convex hull approach is better when we select fewer models to fit our law on. Extended plot in Figure 19.

Prescribing Optimal Tokens Per Parameter by Fitting Power Laws. The final approach described by Hoffmann et al. [2022] is to fit a parametric formula to the loss values with the ansatz

$$L(p,T) = \frac{A}{p^{\alpha}} + \frac{B}{T^{\beta}} + \varepsilon \tag{1}$$

where p is parameter count and T is tokens. We fit our models using L-BGFS [Liu and Nocedal, 1989] with a Huber loss ($\delta = 10^{-4}$) between the empirical log loss and the model prediction, and use multiple initializations following Besiroglu et al. [2024]. We ablate to check that our fitting procedure is robust to the size of the grid of initializations and the choice of delta in Section K.4.

4 Experiments

In Section 4.1, we use our new convex hull fitting method to make a scaling law for the computeoptimal tokens-to-parameters ratio, and compare this to the prescription from our fitted power laws. We show that many design choices such as the learning rate schedule can significantly impact these prescribed scaling laws in Section 4.2. In Section 4.3, we analyze the Gemstones loss values over multiple datasets and connect our analysis to benchmarks. Finally, we perform an analysis over time taken to train instead of over FLOPs in Section 4.4.

4.1 Sizing Up Our Scaling Laws Against Prior Laws and Industry Models

Approach 1. In Figure 3 (row one), we see our validation losses plotted as both a function of FLOPs (left) and GPU hours (right) for the first 100 billion tokens of training. We calculate GPU hours from the average recorded optimizer step time for each model.

Our convex hull fits the data better than prior approaches. Hoffmann et al. [2022]'s Approach 1 creates 250 logarithmically-spaced FLOPs bins per order of magnitude and then uses the models that achieve the best loss in each FLOPs bin to fit the scaling law (a line). However, for our data, their approach does not work very well because it includes many points that are strictly suboptimal with

Table 1: We demonstrate the variability in fitting scaling laws by resampling our data many different ways. The slope can be viewed as the exponent in the power law relationship $parameters = constant \cdot compute^{exponent}$. Grouping by fitting approach and choice to include embeddings, in the final column 'Delta' we show the change in slope produced by the ablations against the corresponding base law fit on the full set of hot data. Values with an absolute magnitude greater than 0.05 are highlighted in orange, and those exceeding 0.1 are highlighted in red. We see that the reduced sampling has a large impact on the slope of the law and that Approach 1 is more sensitive than Approach 3. We plot these prescriptions in Figure 14 and show this table with embeddings excluded from the parameter count in Table 2.

Tokens	Cooldown	LR Ablation	Embeddings	Slope	Delta			
Hoffmann et al. [2022]				0.5126				
Approach 1 (w/ Embeds)								
all	×	×	✓	0.4579				
$\leq 100b$	×	×	✓	0.4994	0.0415			
> 120b	×	X	✓	0.7987	0.3408			
all	×	✓	✓	0.5131	0.0552			
all	✓	×	✓	0.5970	0.1391			
Approach 3 (w/ Embeds)								
all	×	×	✓	0.6965				
$\leq 100b$	×	×	✓	0.6986	0.0021			
> 120b	×	×	✓	0.7515	0.0550			
all	×	✓	✓	0.6740	-0.0225			
all		X	🗸	0.6992	0.0027			
Approach 3 – Chinchilla Reduced Sampling								
all	×	✓	✓ -	0.6328	-0.0636			
all	×	×	✓	0.6315	-0.0649			
Hoffmann et al. [2022]	×	Х	✓	0.6123	0.0997			

respect to the minimal loss envelope. Our convex hull method omits these points, and fits the line with far fewer points.

In Figure 3 (row two), we present the prescriptions from our scaling laws for tokens per parameter. We see that the tokens per parameter prescription of our Approach 1 fitting is close to constant, as in Hoffmann et al. [2022], but suggests a slightly larger optimal tokens per parameter ratio than their law. We extend this plot showing predicted total parameters, tokens, and over multiple ablations in Section K and we give a more detailed plot of each model's individual validation loss in Section J. In Section E, we show a leave-one-out analysis over models when fitting both Approach 1 and 3.

4.2 Fragility and Pitfalls of Scaling Laws

To demonstrate the sensitivity of scaling laws to design choices, we fit laws with various assumptions and model selection rules. To provide compute-optimal parameter count prescriptions, we use equation 4 from Hoffmann et al. [2022], which we restate in Equation (6) for the convenience of the reader.

In Table 1 we show the optimal predictions of multiple possible laws fitted on different subsets of our data. The "slope" column can be viewed as the exponent in the power law relationship between compute and parameters. In the final column "Delta", we show the change in slope produced by the ablations against the corresponding base law fit on the full set of hot data, grouping by fitting approach and choice to include embeddings. We also plot these prescriptions with a FLOPs x-axis in Figure 14.

One particular dimension of variability we wish to highlight briefly here is the interplay between model selection and the derived law. To do this, we select 5 models from Gemstones that have an analogous model in Hoffmann et al. [2022] (using data extracted by Besiroglu et al. [2024]) with similar parameter count and aspect ratio and then we select Gemstones checkpoints with token counts nearly matching the Hoffmann points. We call this "Chinchilla Reduced Sampling" and fit scaling laws to both of these sub-sampled datasets. We find that fitting Hoffmann's data using

this reduced sampling results in an increased slope relative to fitting on all data. Meanwhile this subsampling reduces the slope of the line fit on Gemstones.² This highlights that scaling law fitting can be quite sensitive to seemingly innocuous changes in model selection for both the variable aspect ratio Gemstones models as well as the simpler model family selected by Hoffman.

Between Table 1 and Table 2 we present the complete results from our series of ablations. Table 1 shows the results of fitting laws while including embedding parameter count, which both Pearce and Song [2024] and Porian et al. [2024] find to be a primary explanation of the discrepancies between the prescriptions found by Kaplan et al. [2020] and Hoffmann et al. [2022]. Then in Table 2 we report results when not including the embedding parameter count. We also show the impact of fitting on our cooldown and learning rate ablation datasets in turn, seeing that both choices have a noticeable impact on the prescription for optimal parameter count. Finally, we remove checkpoints from our data to simulate having only trained for 100 billion tokens or only having data for token counts greater than 120 billion, seeing a greater impact than when fitting on our ablation data.

4.3 Modeling Performance on Different Validation Sets and Downstream Benchmarks

In Figure 4 we plot the loss of the $\geq 500M$ Gemstone models on Dolma, FineWeb, FineWeb-Edu and DCLM-baseline data [Soldaini et al., 2024, Penedo et al., 2024, Li et al., 2024b]. We see that when varying the data distribution on which we compute validation loss, although the loss changes for the Gemstones, it is equivalent to a y-axis shift from Dolma; the relative ordering of models remains unchanged. Of particular note is the fact that the deeper models consistently provide a lower loss.

Next, following Penedo et al. [2024], we benchmark our Gemstone models on MMLU [Hendrycks et al., 2020], WinoGrande [Sakaguchi et al., 2021], OpenBook QA [Mihaylov et al., 2018], ARC [Clark et al., 2018], CommonSense QA [Talmor et al., 2018], PIQA [Bisk et al., 2020], SIQA [Sap et al., 2019] and HellaSwag [Zellers et al., 2019]. Specifically, we benchmark the models at 10 billion token intervals during training. We show the benchmark accuracy at selected token counts in Figure 8.

Predicting Benchmark Error We follow Gadre et al. [2024], predicting downstream average top-1 error (Err) across our benchmarks using the recorded validation loss (L), using a function of the form shown in Equation (2) where ϵ, k, γ are fit. In Figure 5, we fit a law to

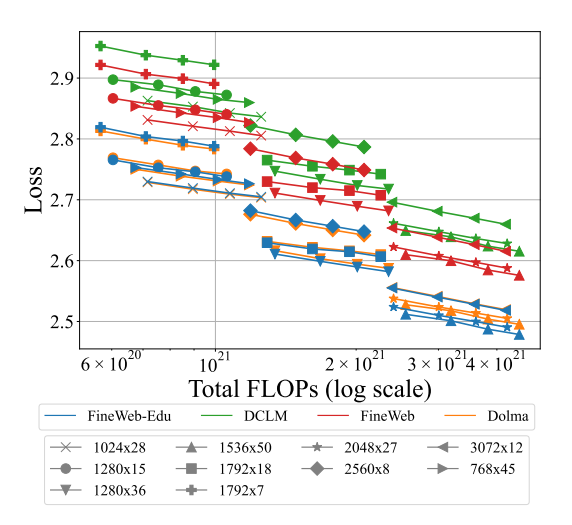


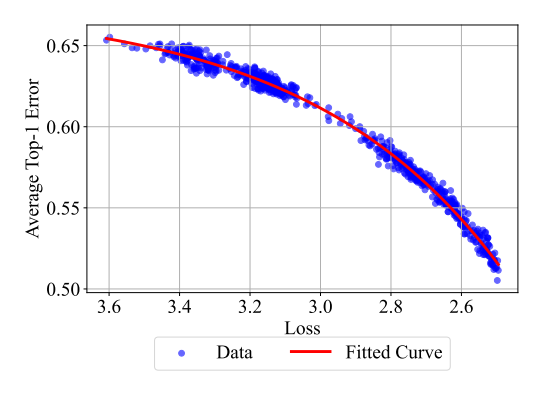
Figure 4: Loss over multiple webtext datasets. We see that the loss value changes for different datasets, including Dolma which we train on. DCLM and FineWeb have higher loss values whereas we measure lower loss values on FineWeb-Edu and Dolma. However, the rank order between models is stable across datasets. This suggests that it may be valid to fit scaling laws on various validation sets without necessarily needing to retrain the underlying models regardless of whether the validation data is i.i.d. with respect to the training distribution.

benchmark results sampled at every 10 billion training tokens, we see that our fitted curve fits the data well. We observe greater variation around the fit compared to Gadre et al. [2024], which we attribute to the considerable differences in the width and depth of the Gemstones models.

Predicting Benchmark Accuracy Following Bhagia et al. [2024], we calculate task loss by taking the loss over the correct answer to each benchmark question and averaging over all questions. We then use this task loss to predict average task accuracy across 4 downstream benchmarks. We find the accuracy of ARC, HellaSwag and MMLU to be most predictable at smaller compute scales and use this subset of benchmarks when fitting scaling laws to predict accuracy. Concurrently, Magnusson

²We note that there are 5 models in this subset for both Hoffmann et al. [2022] and our data, which meets the rule of thumb given by Choshen et al. [2024] for the minimum number of models that should be used to fit a scaling law.

et al. [2025] also observe this pattern across the same set of benchmarks. We predict average task accuracy by fitting a sigmoidal function of the form shown in Equation (3) where a, b, k, l_0 are fit. In Figure 6, we fit a law to benchmark results sampled at every 10 billion training tokens. We see a noisy fit and again suspect this is due to the variation in the Gemstones' width and depth. In Section D, we hold out the 2 billion parameter models and show extrapolation for both benchmark scaling laws and Approach 3 loss predictions.



0.50 0.40 0.35 6.0 5.5 5.0 4.5 4.0 3.5 3.0 Loss Data Fitted Curve

Figure 5: **Benchmark Scaling Law for Error.** We fit a law of the form shown in Equation (2) to benchmark results sampled at every 10 billion tokens and observe a tight fit.

Figure 6: **Benchmark Scaling Law for Accuracy.** We fit a law of the form shown in Equation (3) to benchmark results sampled at every 10 billion tokens for ARC, HellaSwag and MMLU.

$$\operatorname{Err}(L) = \epsilon - k \cdot \exp(-\gamma L)$$
 (2)

$$Acc(L) = \frac{a}{1 + e^{-k(L - L_0)}} + b$$
 (3)

4.4 The Width/Depth vs. Compute/Time Continuum

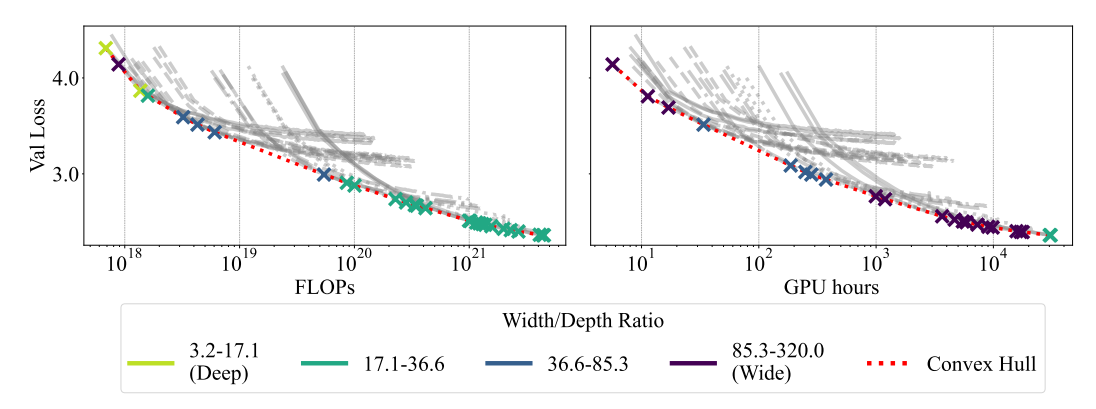


Figure 7: **Approach 1 fitting.** We enlarge and extend Figure 3 (top), highlighting in color the approximate aspect ratio of the vertices that form our convex hull over all 350 billion tokens of training. We see that wider models achieve a lower loss quicker in terms of GPU Hours (right) as the vertices of the convex hull are darker in color. However, deeper models (lighter in color) achieve a lower loss quicker in terms of FLOPs (left).

In the previous section we show how deep models appear to achieve better final loss and accuracy on benchmarks when measured in terms of FLOPs. However, another crucial axis for practitioners to consider is the amount of wall time it takes to train a model. In Figure 7, we visualize in more detail the top of Figure 3, highlighting in color the approximate aspect ratio of the vertices that form our convex hull when fitting. On the left, we see that deep models are able to achieve a lower loss for a given computational budget (FLOPs) and therefore are selected as the vertices of our convex hull when fitting. However, on the right, we see that when the budget is measured in units of computer

time (GPU hours), wider models become more pareto optimal. The concept of "overtraining" is an interesting dimension for further analysis, especially while varying width and depth, as one may be able to overtrain a smaller deep model to reach a low loss value quicker than a larger wider model. We analyze overtraining in greater detail in Section I.

We remark that while in Figure 7 the optimal models with respect to time tend to be the wider ones, this is probably due to our training scheme. Similar to other open-source efforts such as OLMo et al. [2024], we do not make any use of pipeline parallelism, and only employ tensor parallelism (using a hybrid data and tensor parallel algorithm similar to the ubiquitous Fully Sharded Data Parallel strategy). In summary, for standard parallelism implementations, wider models are simply easier to scale, but as a result our observations regarding resource overspending may not generalize to other parallelism strategies. As we open source all artifacts, practitioners can efficiently transform our open source results to suit their training setup. By simply running each model shape for only a handful of steps, recording the step times, updating the step time column in our fitting data and refitting the laws. This means that practitioners can easily transform our GPU Hours analysis to their specific hardware.

Buried Treasure: Unearthing Value in Depth Finally, we plot the average benchmark accuracy (length normalized) of the Gemstones at 200, 250, 300 and 350 billion tokens. Figure 8 shows that the 1B scale models (1280×36 , 2560×8 , and 1792×18) yield increasing accuracy with depth when constrained to approximately the same FLOP budget (vertically aligned points). We see similar patterns with the 768×45 , 1280×15 , 1792×7 , and 1024×28 models, as well as the larger 2B models. This result is hinted at in Table 9 of the Gemma 2 report [Team et al., 2024b], where the authors note that for two models at the 9B scale the deeper model slightly outperforms the wider model across downstream benchmarks, but details of the exact experiment are sparse. Recent work suggests deeper layers in networks "do less" than shallower ones and can be pruned away [Gromov et al., 2024], but our downstream evaluations suggest that there are also advantages to additional model depth. We see similar patterns in the individual performance on each benchmark, and include those charts in Appendix Figure 15.

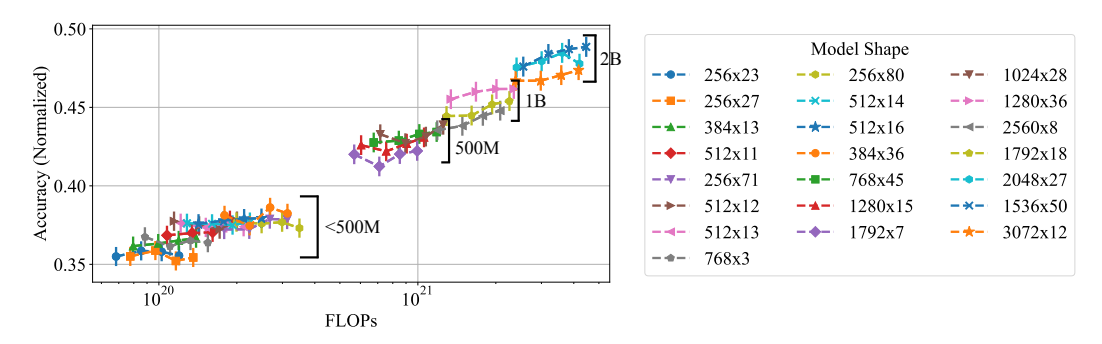


Figure 8: **Benchmark Performance.** We benchmark all models using the 200, 250, 300 and 350 billion token checkpoints. Models show increasing accuracy with depth when constrained to approximately the same FLOP budget (vertically aligned points). This relationship between depth and accuracy can also be observed in many individual benchmarks (Figure 15).

5 Limitations and Conclusions

Altogether, our experiments and analysis demonstrate the impact of often overlooked design choices on scaling law outcomes, the importance of measuring the right type of performance metric, and the nuanced relationship between model width, model depth, computational budget, and training time. We hope this work encourages a rich range of future work based on the suite of open source artifacts we release. Potential avenues for extension include exploring hyperparameters that we kept constant such as the expansion factor of the transformer (the ratio by which the dimensionality of the hidden layer in feed-forward network increased relative to its input dimension), the vocabulary size, the learning rate schedule, and the batch size. Although we endeavor to make our laws as generalizable as possible, we still expect that their applicability declines in training set-ups very different from our own.

Acknowledgments and Disclosure of Funding

We thank (in alphabetical order): Brian Bartoldson, Bhavya Kailkhura, Avi Schwarzschild, Sachin Shah and Abhimanyu Hans for helpful feedback.

An award for computer time was provided by the U.S. Department of Energy's (DOE) Innovative and Novel Computational Impact on Theory and Experiment (INCITE) Program. This research used resources of the Oak Ridge Leadership Computing Facility at the Oak Ridge National Laboratory, which is supported by the Office of Science of the U.S. Department of Energy under Contract No. DE-AC05-00OR22725.

This work was made possible by the ONR MURI program, DAPRA TIAMAT, the National Science Foundation (IIS-2212182), and the NSF TRAILS Institute (2229885). Commercial support was provided by Capital One Bank, the Amazon Research Award program, and Open Philanthropy.

References

- Armen Aghajanyan, Lili Yu, Alexis Conneau, Wei-Ning Hsu, Karen Hambardzumyan, Susan Zhang, Stephen Roller, Naman Goyal, Omer Levy, and Luke Zettlemoyer. Scaling laws for generative mixed-modal language models. In *International Conference on Machine Learning*, pages 265–279. PMLR, 2023.
- Lightning AI. Litgpt. https://github.com/Lightning-AI/litgpt, 2023.
- Joshua Ainslie, James Lee-Thorp, Michiel de Jong, Yury Zemlyanskiy, Federico Lebrón, and Sumit Sanghai. Gqa: Training generalized multi-query transformer models from multi-head checkpoints. *arXiv* preprint arXiv:2305.13245, 2023.
- Ibrahim M Alabdulmohsin, Xiaohua Zhai, Alexander Kolesnikov, and Lucas Beyer. Getting vit in shape: Scaling laws for compute-optimal model design. *Advances in Neural Information Processing Systems*, 36, 2024.
- Jinze Bai, Shuai Bai, Yunfei Chu, Zeyu Cui, Kai Dang, Xiaodong Deng, Yang Fan, Wenbin Ge, Yu Han, Fei Huang, et al. Qwen technical report. *arXiv preprint arXiv:2309.16609*, 2023.
- Yamini Bansal, Behrooz Ghorbani, Ankush Garg, Biao Zhang, Colin Cherry, Behnam Neyshabur, and Orhan Firat. Data scaling laws in nmt: The effect of noise and architecture. In *International Conference on Machine Learning*, pages 1466–1482. PMLR, 2022.
- Tamay Besiroglu, Ege Erdil, Matthew Barnett, and Josh You. Chinchilla scaling: A replication attempt. *arXiv preprint arXiv:2404.10102*, 2024.
- Lucas Beyer, Andreas Steiner, André Susano Pinto, Alexander Kolesnikov, Xiao Wang, Daniel Salz, Maxim Neumann, Ibrahim Alabdulmohsin, Michael Tschannen, Emanuele Bugliarello, et al. Paligemma: A versatile 3b vlm for transfer. *arXiv preprint arXiv:2407.07726*, 2024.
- Akshita Bhagia, Jiacheng Liu, Alexander Wettig, David Heineman, Oyvind Tafjord, Ananya Harsh Jha, Luca Soldaini, Noah A Smith, Dirk Groeneveld, Pang Wei Koh, et al. Establishing task scaling laws via compute-efficient model ladders. *arXiv preprint arXiv:2412.04403*, 2024.
- Xiao Bi, Deli Chen, Guanting Chen, Shanhuang Chen, Damai Dai, Chengqi Deng, Honghui Ding, Kai Dong, Qiushi Du, Zhe Fu, et al. Deepseek llm: Scaling open-source language models with longtermism. *arXiv preprint arXiv:2401.02954*, 2024.
- Stella Biderman, Hailey Schoelkopf, Quentin Gregory Anthony, Herbie Bradley, Kyle O'Brien, Eric Hallahan, Mohammad Aflah Khan, Shivanshu Purohit, USVSN Sai Prashanth, Edward Raff, et al. Pythia: A suite for analyzing large language models across training and scaling. In *International Conference on Machine Learning*, pages 2397–2430. PMLR, 2023.
- Yonatan Bisk, Rowan Zellers, Jianfeng Gao, Yejin Choi, et al. Piqa: Reasoning about physical commonsense in natural language. In *Proceedings of the AAAI conference on artificial intelligence*, volume 34, pages 7432–7439, 2020.

- Blake Bordelon, Lorenzo Noci, Mufan Bill Li, Boris Hanin, and Cengiz Pehlevan. Depthwise hyperparameter transfer in residual networks: Dynamics and scaling limit. In *The Twelfth International Conference on Learning Representations*, 2024. URL https://openreview.net/forum?id= KZJehvRKGD.
- Jason Ross Brown, Yiren Zhao, Ilia Shumailov, and Robert D Mullins. Wide attention is the way forward for transformers? *arXiv preprint arXiv:2210.00640*, 2022.
- Ethan Caballero, Kshitij Gupta, Irina Rish, and David Krueger. Broken neural scaling laws. In *The Eleventh International Conference on Learning Representations*, 2023. URL https://openreview.net/forum?id=sckjveqlCZ.
- Leshem Choshen, Yang Zhang, and Jacob Andreas. A hitchhiker's guide to scaling law estimation, 2024. URL https://arxiv.org/abs/2410.11840.
- Aidan Clark, Diego de Las Casas, Aurelia Guy, Arthur Mensch, Michela Paganini, Jordan Hoffmann, Bogdan Damoc, Blake Hechtman, Trevor Cai, Sebastian Borgeaud, et al. Unified scaling laws for routed language models. In *International conference on machine learning*, pages 4057–4086. PMLR, 2022.
- Peter Clark, Isaac Cowhey, Oren Etzioni, Tushar Khot, Ashish Sabharwal, Carissa Schoenick, and Oyvind Tafjord. Think you have solved question answering? try arc, the ai2 reasoning challenge. arXiv preprint arXiv:1803.05457, 2018.
- Nolan Dey, Gurpreet Gosal, Hemant Khachane, William Marshall, Ribhu Pathria, Marvin Tom, Joel Hestness, et al. Cerebras-gpt: Open compute-optimal language models trained on the cerebras wafer-scale cluster. *arXiv preprint arXiv:2304.03208*, 2023.
- Nolan Dey, Quentin Anthony, and Joel Hestness. The practitioner's guide to the maximal update parameterization, September 2024. URL https://www.cerebras.ai/blog/the-practitioners-guide-to-the-maximal-update-parameterization.
- Nolan Dey, Bin Claire Zhang, Lorenzo Noci, Mufan Li, Blake Bordelon, Shane Bergsma, Cengiz Pehlevan, Boris Hanin, and Joel Hestness. Don't be lazy: Complete enables compute-efficient deep transformers, 2025. URL https://arxiv.org/abs/2505.01618.
- Abhimanyu Dubey, Abhinav Jauhri, Abhinav Pandey, Abhishek Kadian, Ahmad Al-Dahle, Aiesha Letman, Akhil Mathur, Alan Schelten, Amy Yang, Angela Fan, et al. The llama 3 herd of models. arXiv preprint arXiv:2407.21783, 2024.
- Katie E Everett, Lechao Xiao, Mitchell Wortsman, Alexander A Alemi, Roman Novak, Peter J Liu, Izzeddin Gur, Jascha Sohl-Dickstein, Leslie Pack Kaelbling, Jaehoon Lee, and Jeffrey Pennington. Scaling exponents across parameterizations and optimizers. In Ruslan Salakhutdinov, Zico Kolter, Katherine Heller, Adrian Weller, Nuria Oliver, Jonathan Scarlett, and Felix Berkenkamp, editors, Proceedings of the 41st International Conference on Machine Learning, volume 235 of Proceedings of Machine Learning Research, pages 12666–12700. PMLR, 21–27 Jul 2024. URL https://proceedings.mlr.press/v235/everett24a.html.
- Elias Frantar, Carlos Riquelme, Neil Houlsby, Dan Alistarh, and Utku Evci. Scaling laws for sparsely-connected foundation models. *arXiv preprint arXiv:2309.08520*, 2023.
- Samir Yitzhak Gadre, Georgios Smyrnis, Vaishaal Shankar, Suchin Gururangan, Mitchell Wortsman, Rulin Shao, Jean Mercat, Alex Fang, Jeffrey Li, Sedrick Keh, et al. Language models scale reliably with over-training and on downstream tasks. *arXiv preprint arXiv:2403.08540*, 2024.
- Leo Gao, Stella Biderman, Sid Black, Laurence Golding, Travis Hoppe, Charles Foster, Jason Phang, Horace He, Anish Thite, Noa Nabeshima, Shawn Presser, and Connor Leahy. The pile: An 800gb dataset of diverse text for language modeling, 2020. URL https://arxiv.org/abs/2101.00027.
- Leo Gao, Jonathan Tow, Baber Abbasi, Stella Biderman, Sid Black, Anthony DiPofi, Charles Foster, Laurence Golding, Jeffrey Hsu, Alain Le Noac'h, Haonan Li, Kyle McDonell, Niklas Muennighoff, Chris Ociepa, Jason Phang, Laria Reynolds, Hailey Schoelkopf, Aviya Skowron, Lintang Sutawika, Eric Tang, Anish Thite, Ben Wang, Kevin Wang, and Andy Zou. The language model evaluation harness, 07 2024. URL https://zenodo.org/records/12608602.

- Behrooz Ghorbani, Orhan Firat, Markus Freitag, Ankur Bapna, Maxim Krikun, Xavier Garcia, Ciprian Chelba, and Colin Cherry. Scaling laws for neural machine translation. *arXiv* preprint *arXiv*:2109.07740, 2021.
- Mitchell A Gordon, Kevin Duh, and Jared Kaplan. Data and parameter scaling laws for neural machine translation. In *Proceedings of the 2021 Conference on Empirical Methods in Natural Language Processing*, pages 5915–5922, 2021.
- Dirk Groeneveld, Iz Beltagy, Pete Walsh, Akshita Bhagia, Rodney Kinney, Oyvind Tafjord, Ananya Harsh Jha, Hamish Ivison, Ian Magnusson, Yizhong Wang, Shane Arora, David Atkinson, Russell Authur, Khyathi Chandu, Arman Cohan, Jennifer Dumas, Yanai Elazar, Yuling Gu, Jack Hessel, Tushar Khot, William Merrill, Jacob Morrison, Niklas Muennighoff, Aakanksha Naik, Crystal Nam, Matthew E. Peters, Valentina Pyatkin, Abhilasha Ravichander, Dustin Schwenk, Saurabh Shah, Will Smith, Nishant Subramani, Mitchell Wortsman, Pradeep Dasigi, Nathan Lambert, Kyle Richardson, Jesse Dodge, Kyle Lo, Luca Soldaini, Noah A. Smith, and Hannaneh Hajishirzi. Olmo: Accelerating the science of language models. *Preprint*, 2024.
- Andrey Gromov, Kushal Tirumala, Hassan Shapourian, Paolo Glorioso, and Daniel A Roberts. The unreasonable ineffectiveness of the deeper layers. *arXiv* preprint arXiv:2403.17887, 2024.
- Alexander Hägele, Elie Bakouch, Atli Kosson, Loubna Ben Allal, Leandro Von Werra, and Martin Jaggi. Scaling laws and compute-optimal training beyond fixed training durations. *arXiv* preprint arXiv:2405.18392, 2024.
- Soufiane Hayou and Greg Yang. Width and depth limits commute in residual networks. In *International Conference on Machine Learning*, pages 12700–12723. PMLR, 2023.
- Dan Hendrycks, Collin Burns, Steven Basart, Andy Zou, Mantas Mazeika, Dawn Song, and Jacob Steinhardt. Measuring massive multitask language understanding. *arXiv preprint arXiv:2009.03300*, 2020.
- Tom Henighan, Jared Kaplan, Mor Katz, Mark Chen, Christopher Hesse, Jacob Jackson, Heewoo Jun, Tom B Brown, Prafulla Dhariwal, Scott Gray, et al. Scaling laws for autoregressive generative modeling. *arXiv preprint arXiv:2010.14701*, 2020.
- Danny Hernandez, Jared Kaplan, Tom Henighan, and Sam McCandlish. Scaling laws for transfer. *arXiv preprint arXiv:2102.01293*, 2021.
- Jordan Hoffmann, Sebastian Borgeaud, Arthur Mensch, Elena Buchatskaya, Trevor Cai, Eliza Rutherford, Diego de Las Casas, Lisa Anne Hendricks, Johannes Welbl, Aidan Clark, et al. An empirical analysis of compute-optimal large language model training. *Advances in Neural Information Processing Systems*, 35:30016–30030, 2022.
- Shengding Hu, Yuge Tu, Xu Han, Chaoqun He, Ganqu Cui, Xiang Long, Zhi Zheng, Yewei Fang, Yuxiang Huang, Weilin Zhao, et al. Minicpm: Unveiling the potential of small language models with scalable training strategies. *arXiv preprint arXiv:2404.06395*, 2024.
- Itay Inbar and Luke Sernau. Time matters: Scaling laws for any budget, June 2024. URL http://arxiv.org/abs/2406.18922. arXiv:2406.18922 [cs].
- Jared Kaplan, Sam McCandlish, Tom Henighan, Tom B Brown, Benjamin Chess, Rewon Child, Scott Gray, Alec Radford, Jeffrey Wu, and Dario Amodei. Scaling laws for neural language models. arXiv preprint arXiv:2001.08361, 2020.
- Jakub Krajewski, Jan Ludziejewski, Kamil Adamczewski, Maciej Pióro, Michał Krutul, Szymon Antoniak, Kamil Ciebiera, Krystian Król, Tomasz Odrzygóźdź, Piotr Sankowski, et al. Scaling laws for fine-grained mixture of experts. *arXiv preprint arXiv:2402.07871*, 2024.
- Yoav Levine, Noam Wies, Or Sharir, Hofit Bata, and Amnon Shashua. The depth-width interplay in self-attention. In H. Larochelle, M. Ranzato, R. Hadsell, M.F. Balcan, and H. Lin, editors, Advances in Neural Information Processing Systems, volume 33, pages 22640–22651. Curran Associates, Inc., 2020. URL https://proceedings.neurips.cc/paper_files/paper/2020/file/ff4dfdf5904e920ce52b48c1cef97829-Paper.pdf.

- Bozhou Li, Hao Liang, Zimo Meng, and Wentao Zhang. Are bigger encoders always better in vision large models? *arXiv preprint arXiv:2408.00620*, 2024a.
- Jeffrey Li, Alex Fang, Georgios Smyrnis, Maor Ivgi, Matt Jordan, Samir Gadre, Hritik Bansal, Etash Guha, Sedrick Keh, Kushal Arora, Saurabh Garg, Rui Xin, Niklas Muennighoff, Reinhard Heckel, Jean Mercat, Mayee Chen, Suchin Gururangan, Mitchell Wortsman, Alon Albalak, Yonatan Bitton, Marianna Nezhurina, Amro Abbas, Cheng-Yu Hsieh, Dhruba Ghosh, Josh Gardner, Maciej Kilian, Hanlin Zhang, Rulin Shao, Sarah Pratt, Sunny Sanyal, Gabriel Ilharco, Giannis Daras, Kalyani Marathe, Aaron Gokaslan, Jieyu Zhang, Khyathi Chandu, Thao Nguyen, Igor Vasiljevic, Sham Kakade, Shuran Song, Sujay Sanghavi, Fartash Faghri, Sewoong Oh, Luke Zettlemoyer, Kyle Lo, Alaaeldin El-Nouby, Hadi Pouransari, Alexander Toshev, Stephanie Wang, Dirk Groeneveld, Luca Soldaini, Pang Wei Koh, Jenia Jitsev, Thomas Kollar, Alexandros G. Dimakis, Yair Carmon, Achal Dave, Ludwig Schmidt, and Vaishaal Shankar. Datacomp-lm: In search of the next generation of training sets for language models, 2024b.
- Margaret Li, Sneha Kudugunta, and Luke Zettlemoyer. (mis)fitting scaling laws: A survey of scaling law fitting techniques in deep learning. In *The Thirteenth International Conference on Learning Representations*, 2024c. URL https://openreview.net/forum?id=xI71dsS3o4. https://iclr.cc/virtual/2025/poster/27795.
- Zhengyang Liang, Hao He, Ceyuan Yang, and Bo Dai. Scaling laws for diffusion transformers. *arXiv* preprint arXiv:2410.08184, 2024.
- Dong C. Liu and Jorge Nocedal. On the limited memory bfgs method for large scale optimization. *Mathematical Programming*, 45(1):503–528, 1989. doi: 10.1007/BF01589116.
- Ilya Loshchilov and Frank Hutter. Decoupled weight decay regularization. *arXiv preprint* arXiv:1711.05101, 2017.
- Ian Magnusson, Nguyen Tai, Ben Bogin, David Heineman, Jena D Hwang, Luca Soldaini, Akshita Bhagia, Jiacheng Liu, Dirk Groeneveld, Oyvind Tafjord, et al. Datadecide: How to predict best pretraining data with small experiments. *arXiv preprint arXiv:2504.11393*, 2025.
- Todor Mihaylov, Peter Clark, Tushar Khot, and Ashish Sabharwal. Can a suit of armor conduct electricity? a new dataset for open book question answering. *arXiv preprint arXiv:1809.02789*, 2018.
- Niklas Muennighoff, Alexander Rush, Boaz Barak, Teven Le Scao, Nouamane Tazi, Aleksandra Piktus, Sampo Pyysalo, Thomas Wolf, and Colin A Raffel. Scaling data-constrained language models. *Advances in Neural Information Processing Systems*, 36:50358–50376, 2023.
- Team OLMo, Pete Walsh, Luca Soldaini, Dirk Groeneveld, Kyle Lo, Shane Arora, Akshita Bhagia, Yuling Gu, Shengyi Huang, Matt Jordan, et al. 2 olmo 2 furious. *arXiv preprint arXiv:2501.00656*, 2024.
- Tim Pearce and Jinyeop Song. Reconciling kaplan and chinchilla scaling laws, 2024. URL https://arxiv.org/abs/2406.12907.
- Guilherme Penedo, Hynek Kydlíček, Anton Lozhkov, Margaret Mitchell, Colin A Raffel, Leandro Von Werra, Thomas Wolf, et al. The fineweb datasets: Decanting the web for the finest text data at scale. *Advances in Neural Information Processing Systems*, 37:30811–30849, 2024.
- Jackson Petty, Sjoerd van Steenkiste, Ishita Dasgupta, Fei Sha, Dan Garrette, and Tal Linzen. The impact of depth on compositional generalization in transformer language models, 2024. URL https://arxiv.org/abs/2310.19956.
- Tomer Porian, Mitchell Wortsman, Jenia Jitsev, Ludwig Schmidt, and Yair Carmon. Resolving discrepancies in compute-optimal scaling of language models. arXiv preprint arXiv:2406.19146, 2024.
- Yangjun Ruan, Chris J. Maddison, and Tatsunori Hashimoto. Observational scaling laws and the predictability of language model performance, 2024. URL https://arxiv.org/abs/2405.10938.

- Keisuke Sakaguchi, Ronan Le Bras, Chandra Bhagavatula, and Yejin Choi. Winogrande: An adversarial winograd schema challenge at scale. Communications of the ACM, 64(9):99–106, 2021.
- Maarten Sap, Hannah Rashkin, Derek Chen, Ronan LeBras, and Yejin Choi. Socialiqa: Commonsense reasoning about social interactions. *arXiv preprint arXiv:1904.09728*, 2019.
- Siddharth Singh and Abhinav Bhatele. Axonn: An asynchronous, message-driven parallel framework for extreme-scale deep learning. In 2022 IEEE International Parallel and Distributed Processing Symposium (IPDPS), pages 606–616, 2022. doi: 10.1109/IPDPS53621.2022.00065.
- Siddharth Singh, Prajwal Singhania, Aditya K. Ranjan, Zack Sating, and Abhinav Bhatele. A 4d hybrid algorithm to scale parallel training to thousands of gpus, 2024. URL https://arxiv.org/abs/2305.13525.
- Luca Soldaini, Rodney Kinney, Akshita Bhagia, Dustin Schwenk, David Atkinson, Russell Authur, Ben Bogin, Khyathi Chandu, Jennifer Dumas, Yanai Elazar, Valentin Hofmann, Ananya Harsh Jha, Sachin Kumar, Li Lucy, Xinxi Lyu, Nathan Lambert, Ian Magnusson, Jacob Morrison, Niklas Muennighoff, Aakanksha Naik, Crystal Nam, Matthew E. Peters, Abhilasha Ravichander, Kyle Richardson, Zejiang Shen, Emma Strubell, Nishant Subramani, Oyvind Tafjord, Pete Walsh, Luke Zettlemoyer, Noah A. Smith, Hannaneh Hajishirzi, Iz Beltagy, Dirk Groeneveld, Jesse Dodge, and Kyle Lo. Dolma: an Open Corpus of Three Trillion Tokens for Language Model Pretraining Research. *arXiv preprint*, 2024.
- Alon Talmor, Jonathan Herzig, Nicholas Lourie, and Jonathan Berant. Commonsenseqa: A question answering challenge targeting commonsense knowledge. *arXiv preprint arXiv:1811.00937*, 2018.
- Yi Tay, Mostafa Dehghani, Jinfeng Rao, William Fedus, Samira Abnar, Hyung Won Chung, Sharan Narang, Dani Yogatama, Ashish Vaswani, and Donald Metzler. Scale efficiently: Insights from pretraining and finetuning transformers. In *International Conference on Learning Representations*, 2022. URL https://openreview.net/forum?id=f20YVDyfIB.
- Gemma Team, Thomas Mesnard, Cassidy Hardin, Robert Dadashi, Surya Bhupatiraju, Shreya Pathak, Laurent Sifre, Morgane Rivière, Mihir Sanjay Kale, Juliette Love, et al. Gemma: Open models based on gemini research and technology. *arXiv preprint arXiv:2403.08295*, 2024a.
- Gemma Team, Morgane Riviere, Shreya Pathak, Pier Giuseppe Sessa, Cassidy Hardin, Surya Bhupatiraju, Léonard Hussenot, Thomas Mesnard, Bobak Shahriari, Alexandre Ramé, et al. Gemma 2: Improving open language models at a practical size. *arXiv preprint arXiv:2408.00118*, 2024b.
- Hugo Touvron, Louis Martin, Kevin Stone, Peter Albert, Amjad Almahairi, Yasmine Babaei, Nikolay Bashlykov, Soumya Batra, Prajjwal Bhargava, Shruti Bhosale, et al. Llama 2: Open foundation and fine-tuned chat models. arXiv preprint arXiv:2307.09288, 2023.
- Thomas Wolf, Lysandre Debut, Victor Sanh, Julien Chaumond, Clement Delangue, Anthony Moi, Pierric Cistac, Tim Rault, Rémi Louf, Morgan Funtowicz, Joe Davison, Sam Shleifer, Patrick von Platen, Clara Ma, Yacine Jernite, Julien Plu, Canwen Xu, Teven Le Scao, Sylvain Gugger, Mariama Drame, Quentin Lhoest, and Alexander M. Rush. Huggingface's transformers: State-of-the-art natural language processing, 2020. URL https://arxiv.org/abs/1910.03771.
- An Yang, Baosong Yang, Binyuan Hui, Bo Zheng, Bowen Yu, Chang Zhou, Chengpeng Li, Chengyuan Li, Dayiheng Liu, Fei Huang, Guanting Dong, Haoran Wei, Huan Lin, Jialong Tang, Jialin Wang, Jian Yang, Jianhong Tu, Jianwei Zhang, Jianxin Ma, Jianxin Yang, Jin Xu, Jingren Zhou, Jinze Bai, Jinzheng He, Junyang Lin, Kai Dang, Keming Lu, Keqin Chen, Kexin Yang, Mei Li, Mingfeng Xue, Na Ni, Pei Zhang, Peng Wang, Ru Peng, Rui Men, Ruize Gao, Runji Lin, Shijie Wang, Shuai Bai, Sinan Tan, Tianhang Zhu, Tianhao Li, Tianyu Liu, Wenbin Ge, Xiaodong Deng, Xiaohuan Zhou, Xingzhang Ren, Xinyu Zhang, Xipin Wei, Xuancheng Ren, Xuejing Liu, Yang Fan, Yang Yao, Yichang Zhang, Yu Wan, Yunfei Chu, Yuqiong Liu, Zeyu Cui, Zhenru Zhang, Zhifang Guo, and Zhihao Fan. Qwen2 technical report, 2024a. URL https://arxiv.org/abs/2407.10671.

- An Yang, Baosong Yang, Beichen Zhang, Binyuan Hui, Bo Zheng, Bowen Yu, Chengyuan Li, Dayiheng Liu, Fei Huang, Haoran Wei, et al. Qwen2.5 technical report. *arXiv preprint arXiv:2412.15115*, 2024b.
- Ge Yang, Edward Hu, Igor Babuschkin, Szymon Sidor, Xiaodong Liu, David Farhi, Nick Ryder, Jakub Pachocki, Weizhu Chen, and Jianfeng Gao. Tuning large neural networks via zero-shot hyperparameter transfer. In M. Ranzato, A. Beygelzimer, Y. Dauphin, P.S. Liang, and J. Wortman Vaughan, editors, *Advances in Neural Information Processing Systems*, volume 34, pages 17084–17097. Curran Associates, Inc., 2021. URL https://proceedings.neurips.cc/paper_files/paper/2021/file/8df7c2e3c3c3be098ef7b382bd2c37ba-Paper.pdf.
- Greg Yang and Edward J. Hu. Tensor programs iv: Feature learning in infinite-width neural networks. In Marina Meila and Tong Zhang, editors, *Proceedings of the 38th International Conference on Machine Learning*, volume 139 of *Proceedings of Machine Learning Research*, pages 11727–11737. PMLR, 18–24 Jul 2021.
- Greg Yang, Dingli Yu, Chen Zhu, and Soufiane Hayou. Tensor programs vi: Feature learning in infinite-depth neural networks. *arXiv preprint arXiv:2310.02244*, 2023.
- Longfei Yun, Yonghao Zhuang, Yao Fu, Eric P Xing, and Hao Zhang. Toward inference-optimal mixture-of-expert large language models. *arXiv preprint arXiv:2404.02852*, 2024.
- Rowan Zellers, Ari Holtzman, Yonatan Bisk, Ali Farhadi, and Yejin Choi. Hellaswag: Can a machine really finish your sentence? *arXiv preprint arXiv:1905.07830*, 2019.
- Biao Zhang, Behrooz Ghorbani, Ankur Bapna, Yong Cheng, Xavier Garcia, Jonathan Shen, and Orhan Firat. Examining scaling and transfer of language model architectures for machine translation. In *International Conference on Machine Learning*, pages 26176–26192. PMLR, 2022.
- Biao Zhang, Zhongtao Liu, Colin Cherry, and Orhan Firat. When scaling meets Ilm finetuning: The effect of data, model and finetuning method. *arXiv preprint arXiv:2402.17193*, 2024.
- Jingwei Zuo, Maksim Velikanov, Ilyas Chahed, Younes Belkada, Dhia Eddine Rhayem, Guillaume Kunsch, Hakim Hacid, Hamza Yous, Brahim Farhat, Ibrahim Khadraoui, et al. Falcon-h1: A family of hybrid-head language models redefining efficiency and performance. arXiv preprint arXiv:2507.22448, 2025.

A Model Implementation Details

All models have a head size of 128 because 256 is the maximum head dimension supported by the AMD implementation of Flash Attention 2 we utilize and we constrain our search to models with > 1 attention heads. We assume the simple convention of the Llama series where the head dimension is always the embedding dimension divided by the number of heads, implying that the embedding dimension (width) must be divisible by 128. Following conventions from the Gemma suite, we constrain the head count to be even to enable Grouped Query Attention [Ainslie et al., 2023] with a query to key ratio of 2:1 and we fix the intermediate size to be $4\times$ the width of the model. We choose our vocabulary size to match the 50,304 tokens in the Pythia tokenizer. While many of the architecture choices mirror those from Gemma, for simplicity we do not use logit softcapping nor do we tie the embedding and language modeling head weight matrices.

A.1 Optimal Learning Rates for Gemstones

Training models across diverse shapes and scales requires learning rates that ensure both stability and near-optimal performance. Suboptimal learning rates risk misrepresenting scaling laws, as they could conflate architectural preferences with hyperparameter sensitivity. For the Gemstone models—varying in width, depth, and size—we address this challenge through a unified learning rate scaling rule and a parameter initialization scheme tailored for stability.

Unified Learning Rate Scaling Rule Existing scaling rules prescribe learning rates (lr) as $lr_{\rm base}/{\rm width}$ for width scaling or $lr_{\rm base}/\sqrt{{\rm depth}}$ for depth scaling. Since Gemstone models vary both dimensions, we propose a hybrid rule: $lr_{\rm eff} = lr_{\rm base}/({\rm width} \times \sqrt{{\rm depth}})$ This accounts for the compounding effect of gradient dynamics across width and depth, balancing update magnitudes during optimization.

Empirical Validation To validate $lr_{\rm base}$, we stress-test four extreme model shapes: wide (64 layers, 768 width) and deep (128 layers, 512 width) at 100M and 2B parameter scales. Each is trained for 1k steps with a batch size of 2048 and context length of 2048 (4.2B tokens). We sweep $lr_{\rm eff}$ from 10^{-4} to 5×10^{-2} . As shown in Figure 9 (left), optimal $lr_{\rm eff}$ varies widely across architectural shape. However, rescaling the x-axis by width $\times \sqrt{\rm depth}$ collapses all curves onto a shared trend, revealing $lr_{\rm base}=5$ as the consistent optimum (right panel). This confirms our rule's efficacy for width-depth transfer.

Flaws in the Gemstones. While $lr_{\rm base}=5$ achieves stable training for most models under the scheme described above, wider architectures (e.g., 256 width-depth ratio) occasionally exhibit loss spikes nonetheless. Despite these instabilities, via rollbacks and minor modifications to the learning rates for the most extreme models, all models in the suite are trained to 350B tokens without divergence. We discuss these issues and our solutions further in Section J.2.

Ablation Study To assess sensitivity to $lr_{\rm base}$, we replicate training for a subset of models with $lr_{\rm base}=2.5$ (e.g. dividing $lr_{\rm eff}$ by 2). While losses are marginally higher, scaling law fits remain robust, suggesting our conclusions are not artifacts of aggressive learning rates.

Scalable Parameter Initialization Rules. Finally, stable training across model shapes and scales also requires model specific tweaks to parameter initialization Yang et al. [2021]. Following OLMo(1) [Groeneveld et al., 2024], we apply a parameter initialization strategy intended to enable stable training and learning rate transfer across scales. We initialize all parameters as truncated normal ($\mu=0, a=-3\cdot\sigma, b=3\cdot\sigma$) with modified variances dependent on the parameter type. We use $\sigma=1/\sqrt{\text{width}}$ except for the attention projections which are initialized as $\sigma=1/\sqrt{2\cdot\text{width}\cdot(l+1)}$ and the MLP projections as $\sigma=1/\sqrt{2\cdot(4\times\text{width})\cdot(l+1)}$ where in each case l is the layer index (not the total model depth) and the $4\times$ factor comes from the relation of width to MLP intermediate dimension.

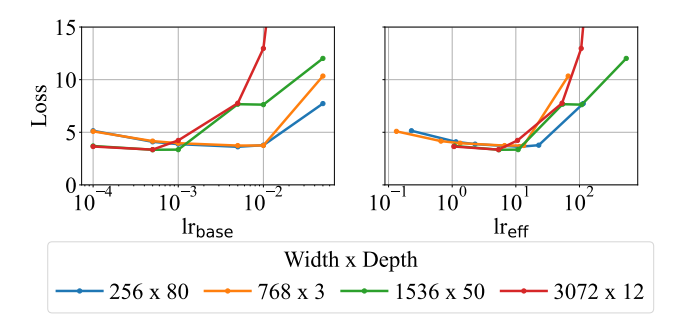


Figure 9: Learning rate scaling is necessary for width-depth transfer. Left: Preliminary training runs with initialization rules active, but no learning rate scaling. Right: Same data, but with x-axis rescaled to simulate the application of learning rate scaling with $lr_{\text{base}} = lr_{\text{eff}} \times (\text{width} \times \sqrt{\text{depth}})$.

A.2 Software and Data

We train all models using a fork of litgpt [AI, 2023] enhanced with AxoNN [Singh and Bhatele, 2022, Singh et al., 2024] tensor parallelism. We open source all models used in our analysis to Hugging Face [Wolf et al., 2020] and the logging from training on Weights and Biases in json format.

B Extended Related Works

Scaling laws are broadly applied to many areas of machine learning, such as machine translation. Ghorbani et al. [2021] split the parameters term into two, one for each of encoder and decoder, and similarly to Gordon et al. [2021] analyze the relationship between BLEU scores and scaling laws. Zhang et al. [2022] and Bansal et al. [2022] study the impact of architecture choice on the scaling law, finding increasing data or parameters can compensate for worse architectural decisions.

There are multiple works analyzing whether scaling laws can be used to predict downstream performance. Ruan et al. [2024] show that scaling laws can be predictive of benchmark performance. Caballero et al. [2023] observe that traditional scaling laws cannot capture complex behaviors like non-monotonic trends nor inflection points. They propose broken scaling laws—a piecewise or smoothly broken power law—that better predicts performance of both upstream and downstream tasks.

Scaling laws have also been applied to sparse architectures. Clark et al. [2022] analyze how the number of experts can be used in the law, studying both linear and quadratic interactions for many types of routing models. Yun et al. [2024] extend this, analyzing the trade offs between optimal training and optimal inference. Krajewski et al. [2024] find that with optimal settings a Mixture of Experts model always outperforms a transformer model at any computational budget. Frantar et al. [2023] focus on weight sparsity within foundation models, adding a multiplicative parameter on the parameters term in the law. Model shape has also been analyzed for sparse mixture of expert models and in the context of finetuning. Krajewski et al. [2024] use the ratio between the standard feed-forward hidden dimension and the hidden dimension of an individual expert to allow their law for mixture of expert models to predict the width of the experts.

These techniques are not limited to generative text modeling only; they have also been applied to multi-model models. Henighan et al. [2020] find optimal model size can be described as a power law for model modeling including images and video. The authors also find that model size does not help 'strong generalization' for problem solving. Aghajanyan et al. [2023] analyze text, images, code and speech, presenting a scaling law to describe the competition between these modalities and describe a regime for optimal hyperparameter transfer from the unimodal to multimodal regimes. Liang et al. [2024] look at scaling laws for diffusion transformer models. Li et al. [2024a] analyze scaling laws for vision encoder commonly used to encode image inputs for transformer model backbones, finding increasing the size of the encoder alone can lead to performance degradation in some cases.

Further analyses using scaling laws have extended to analyzing finetuning and data limited scaling. Hernandez et al. [2021] find that finetuning is much more compute efficient when the pretraining ignored. Zhang et al. [2024] study parameter efficient finetuning regimes find a multiplicative law is better for the finetuning setting than the classical additive law used by others. Muennighoff et al.

[2023] analyze the data constrained training regimes, finding epoching data up to four times is as good as training on deduplicated data in terms of reducing loss.

Zero-shot Hyperparameter Transfer The ability to train a series of models with extremely different parameter counts is an implicit requirement of any scaling law analysis. Work on zero-shot hyperparameter transfer across transformer model *widths* is mature [Yang et al., 2021, Everett et al., 2024, Hayou and Yang, 2023, Dey et al., 2024]. Achieving transfer across diverse model *depths* is less well studied, especially in transformer language models [Bordelon et al., 2024, Yang and Hu, 2021, Yang et al., 2023]. While Yang et al. [2023] argue that depth transfer requires scaling in $1/\sqrt{L}$ because this is the unique regime with maximum feature diversity, more recently Dey et al. [2025] argue that instead the scaling should be in 1/L.

B.1 Chinchilla Equation 4

Hoffmann et al. [2022] use the variable names N and D for the number of parameters and number of tokens respectively, defining their parameterized form as:

$$\hat{L}(N,D) \triangleq E + \frac{A}{N^{\alpha}} + \frac{B}{D^{\beta}},$$
 (4)

Equation 4 of Hoffmann et al. [2022] is defined as:

$$N_{opt}(C) = G\left(\frac{C}{6}\right)^a, \quad D_{opt}(C) = G^{-1}\left(\frac{C}{6}\right)^b, \tag{5}$$

where
$$G = \left(\frac{\alpha A}{\beta B}\right)^{\frac{1}{\alpha + \beta}}$$
, $a = \frac{\beta}{\alpha + \beta}$, and $b = \frac{\alpha}{\alpha + \beta}$. (6)

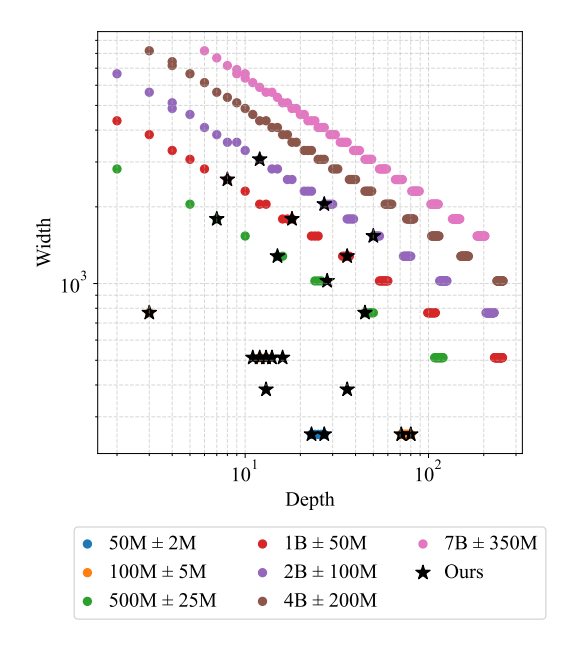


Figure 10: All possible model shapes we could have chosen based on our architecture within $\pm 5\%$ are shown as circles. The points we selected are highlighted as stars, including the two extra points we select to have four models of width 512.

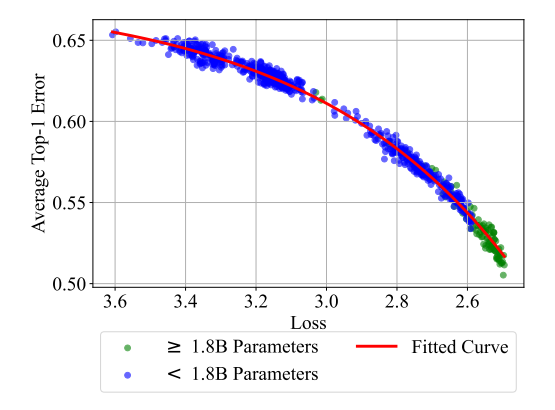
C Data Sampling

We plot the entire space of all possible models subject to our design constraints discussed in Figure 10. While exploring the impact of finer grained depth differences during our experiments, we decided

to add two additional models slightly outside the $\pm 5\%$ tolerance band at the 100M scale; for width=512, in addition to the originally chosen depths of 12 and 13, we added 11 and 14; these appear as a dense collection of 4 points at the same width.

D Extrapolation to Larger Models

To quantify the robustness of our scaling laws to changes in model scale, we perform two types of extrapolation analyses. In the first experiment, we hold out the "2B" parameter models, fit scaling laws to the samller models, and then test the extrapolation performance of the fitted law. Due to the 10% tolerance margin in our parameter count strata, in actuality we fit benchmark scaling laws using models with less than 1.8B parameters and extrapolate to models with more than 1.8B parameters. In Figure 11 we see that extrapolating to predict error offers a much better fit than we see in Figure 12 when predicting accuracy.



0.50
0.45
0.40
0.35
6.0 5.5 5.0 4.5 4.0 3.5 3.0
Loss

< 1.8B Parameters

≥ 1.8B Parameters

→ Fitted Curve

Figure 11: **Benchmark Scaling Law for Error.** We fit a law of the form shown in Equation (2) to benchmark results sampled at every 10 billion tokens using models with less than 1.8B parameters and observe a tight fit when extrapolating to models with more than 1.8B parameters.

Figure 12: **Benchmark Scaling Law for Accuracy.** We fit a law of the form shown in Equation (3) to benchmark results sampled at every 10 billion tokens for ARC, HellaSwag and MMLU using models with less than 1.8B parameters and observe a poor fit when extrapolating to models with more than 1.8B parameters.

In a second type of experiment, we again analyze extrapolation as a function of model size but this time quantifying prescription robustness in terms of estimated versus actual validation loss (using approach 3). Following Choshen et al. [2024], we report the mean absolute relative error (ARE) over the last 30% of training tokens (250b to 350b tokens for Gemstone models). We find the ARE when fitting on all checkpoints and then testing on models with more than 1.8B parameters is 0.68%. When only fitting on models with less than 1.8B parameters and extrapolating to models with more than 1.8B parameters, the ARE is 0.63%. Choshen et al. [2024] find ARE's of up to 4% are typically used to distinguish between modeling choices, implying that our extrapolation error is well within the acceptable range.

E Leave-One-model-Out Analysis

To evaluate how robust our scaling laws are to a different aspect of our experimental design, we estimate the variability in our fitting process caused by our model selection using a leave-one-out analysis. In Figure 13 we re-fit the same scaling law multiple times leaving each one of the model shapes out in turn using both Approach 1 and Approach 3. We visualize these results by plotting the minimum and maximum tokens per parameter ratios yielded across all leave-one-out trials along with the prescription based on all data (bounds of the gray shaded region vs the green line). While the implications of the precise min/max values are somewhat up to interpretation, compared to the

difference between our fit, Kaplan's, and Chinchilla's, the relative narrowness of the gray region suggests that any disagreement in tokens per parameter prescription we find versus prior work is unlikely to simply be an artifact of (our) specific model selection. Finally, comparing the left and right sides of Figure 13, the smaller gray region in the former suggests that Approach 1 is less sensitive to this model re-sampling process than Approach 3. We hypothesize that at least some of this increased robustness in fit can be attributed to our novel variance-reducing convex hull method applied in Approach 1.

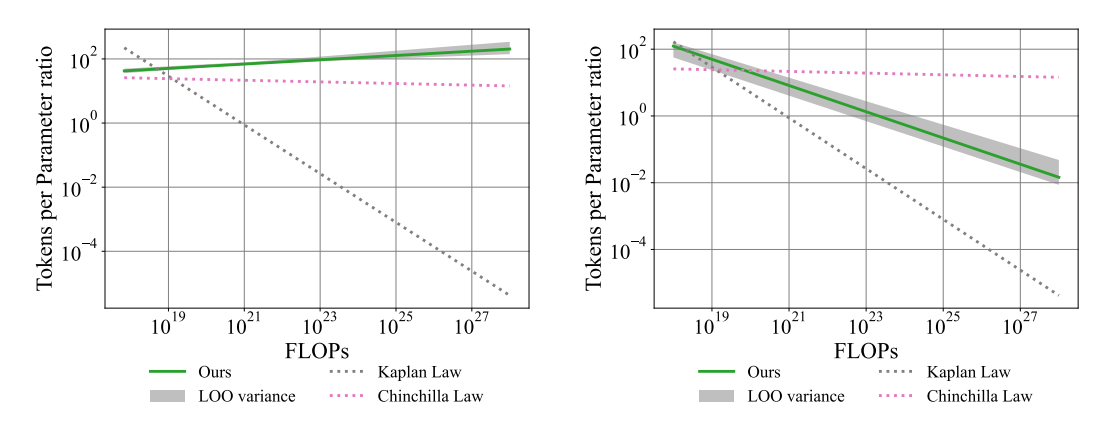


Figure 13: **Leave-One-Out Validation.** We leave each model out and refit the law to obtain the gray shaded region (min/max ratio across all trials) and compare it with the law fit to all data in green. **Left**) shows the result when Approach 1 is used, and **right**) shows the result of using Approach 3.

F Variability in fitting

In Table 2, we show a similar table to Table 1 but exclude embeddings from the parameter count in the fitting process. We also visualize all fitted lines in Figure 14.

Table 2: We demonstrate the variability in fitting scaling laws by resampling our data many different ways. The slope can be viewed as the exponent in the power law relationship $parameters = constant \cdot compute^{exponent}$. Grouping by fitting approach and choice to include embeddings, in the final column 'Delta' we show the change in slope produced by the ablations against the corresponding base law fit on the full set of hot data. Values with an absolute magnitude greater than 0.05 are highlighted in orange, and those exceeding 0.1 are highlighted in red. We see that the reduced sampling has a large impact on the slope of the law and that Approach 1 is more sensitive than Approach 3. We plot these prescriptions in Figure 14 and show this table with embeddings included in the parameter count in Table 1.

Tokens	Cooldown	LR Ablation	Embeddings	Slope	Delta			
Kaplan et al. [2020]				0.7300				
Approach 1 (no Embeds)								
all	X	X	X	0.5689				
$\leq 100b$	X	X	X	0.6269	0.0579			
> 120b	X	X	X	0.9666	0.3977			
all	X	✓	X	0.6224	0.0535			
all	✓	×	×	0.7242	0.1552			
Approach 3 (no Embeds)								
all	X	X	X	0.7141				
$\leq 100b$	X	X	X	0.7030	-0.0111			
> 120b	X	X	X	0.7350	0.0209			
all	X	✓	X	0.6929	-0.0211			
all	✓	Х	Х	0.7104	-0.0037			

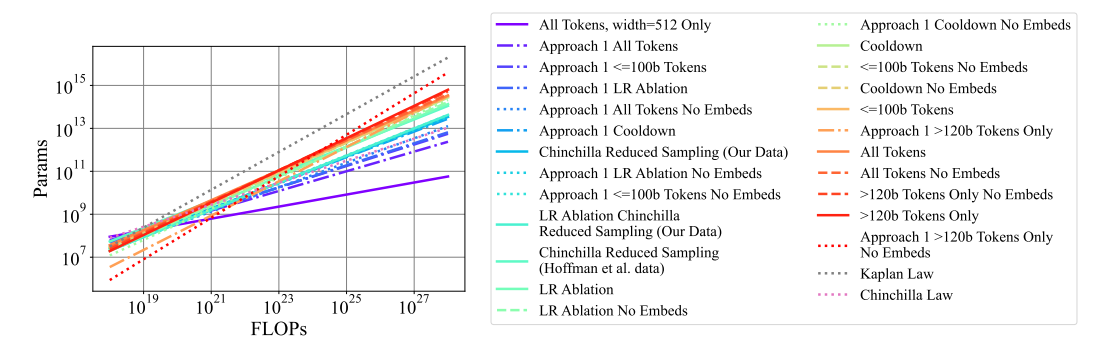


Figure 14: We demonstrate the variability in fitting scaling laws by resampling our data many different ways. We label prescriptions found using Approach 1 with "Approach 1" in the legend, otherwise approach 3 is used. All tokens counts available are used to fit the laws unless stated otherwise in the legend, for example $\leq 100B$ means that only token counts less than or equal to 100B are used in fitting.

No Embeds: Embedding parameters are not counted when fitting these laws.

Cooldown: Only data from the cooldown ablation is used to fit this law.

LR Ablation: Only data from the learning rate ablation training runs, where the learning rate is halved, is used to fit these laws.

width=512 Only: Only models with width 512 are used to fit these laws.

Chinchilla Reduced Sampling: We subsample our data to be as close as possible to the token counts and model sizes that Hoffmann et al. [2022] use to fit their scaling laws and also fit new scaling laws on this subset of Hoffmann et al. [2022] data. Details in Section 4.2.

G Individual Benchmark Results

In Figure 15, we see zero-shot MMLU scores of our larger models are quite non-trivial at 28% - 33%, despite being trained on an open dataset, without a cooldown period, or any sort of post-training.

H The Price of Stepping Off the Scaling Law

By analyzing the cost of stepping off of the scaling law, we find that some kinds of design errors are more damaging than others. We also find that training on more tokens than is strictly recommended (aka "overtraining") is typically quite efficient in terms of pushing down loss.

If You Value Your Time, Train Wide Models. We first show that in our training setup, training wider models is far more efficient than training deep models. In Figure 16, we reflect on the consequences of suboptimal architectural choices, by considering how much of a given resource—FLOPs or GPU hours—would be "overspent" to reach any target loss value with the plotted architecture rather than the prescribed width and depth. We find that choosing to train "skinny" models (top left) wastes many FLOPs and GPU hours. The scale of overspend is quite different however, with the least efficient models only overspending about 50% on FLOPs but wasting more than 200% of the GPU hours spent by the best configuration. In other words, in the time taken to train a single (very) suboptimal model to the desired loss value, one could train three optimal-width-depth models. We note that while the time-optimal models tend to be the wider ones, this is probably due to our training scheme. Similar to other open-source efforts such as OLMo et al. [2024], we do not make any use of pipeline parallelism. In summary, for standard parallelism implementations, wider models are simply easier to scale, but as a result our observations regarding resource overspending may not generalize to other parallelism strategies.

I Scaling Laws Predict That Overtraining Is Efficient.

Similarly to Gadre et al. [2024], we can shift optimal points to simulate overtraining. To do this, we fix a FLOP budget and trace out a path of model sizes and corresponding token counts to remain

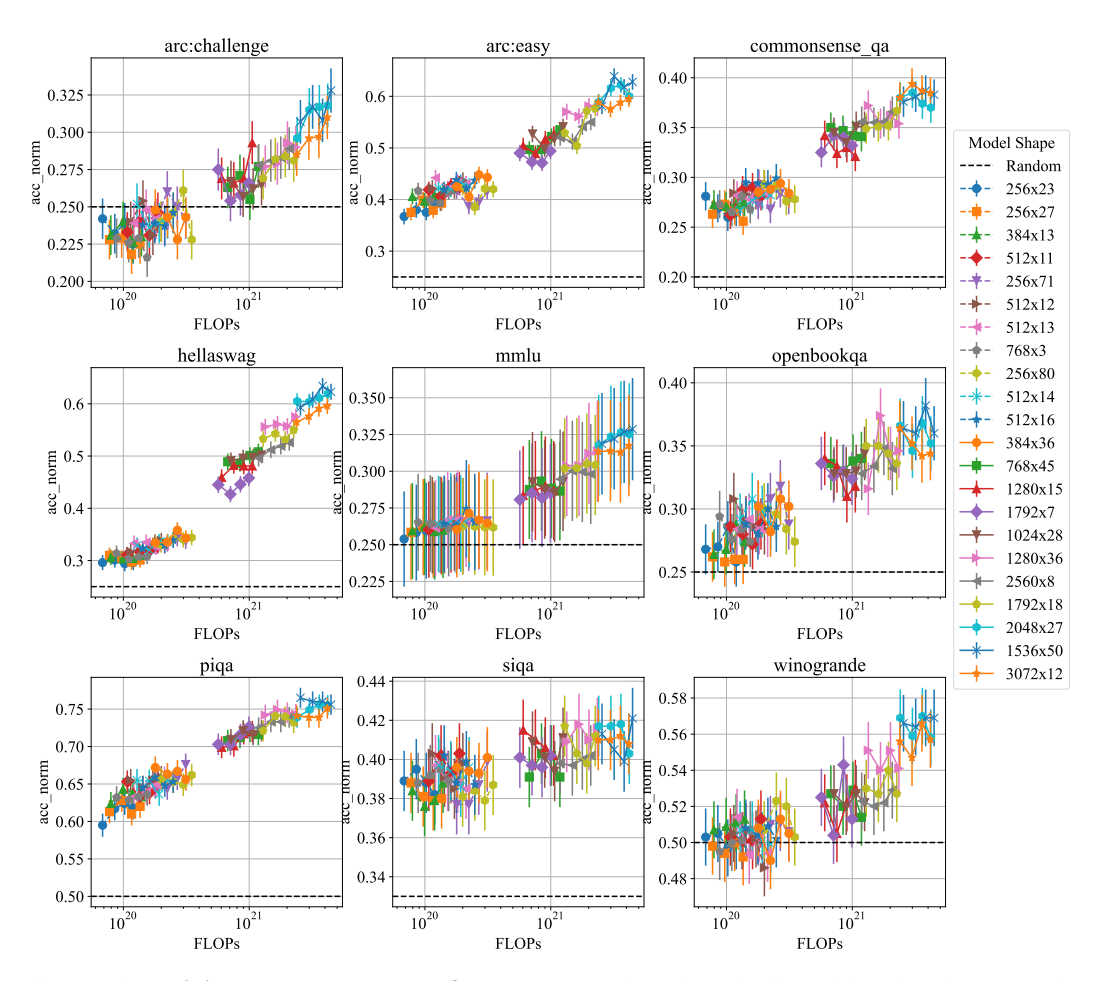


Figure 15: **Individual benchmark performance.** We benchmark all models using the 200, 250, 300, and 350B token checkpoints, converting this to FLOPs using the formula shown in Section L. Models show increasing accuracy with depth when constrained to approximately the same FLOP budget (vertically aligned points) on many benchmarks. We plot the average benchmark accuracy in Figure 8.

within that budget. For each model size and token count, we record the "overtraining factor," which is the selected number of training tokens divided by the optimal number of tokens for that model shape. An overtraining factor of less than one corresponds to undertraining the model, and a factor greater than one represents overtraining. We show the results of this process in Figure 17. We see that overtraining does increase predicted loss at a given FLOP count but that these curves are actually quite flat. We include the loss values of open source models on our own validation set to allow readers to contextualize the y-axis values. Especially at high FLOP counts, our laws predict overtraining becomes quite efficient in that it results in fairly small elevations in loss for a relatively large reduction in model size.

Industry models often use fewer parameters and train on more tokens than prescribed in prior work. We find the impact of overtraining a smaller model on predicted loss to be small. Combining this with Figure 16, where wider models are predicted to be optimal in terms of GPU hours, reinforces the message that FLOPs optimality is not the end of the story for training models. Trading some FLOPs optimality for time optimality necessarily means overtraining, but Figure 17 suggests the difference is marginal. We believe this combined evidence makes significant progress towards explaining the differences between the prescriptions found in prior work and training choices observed in industry.

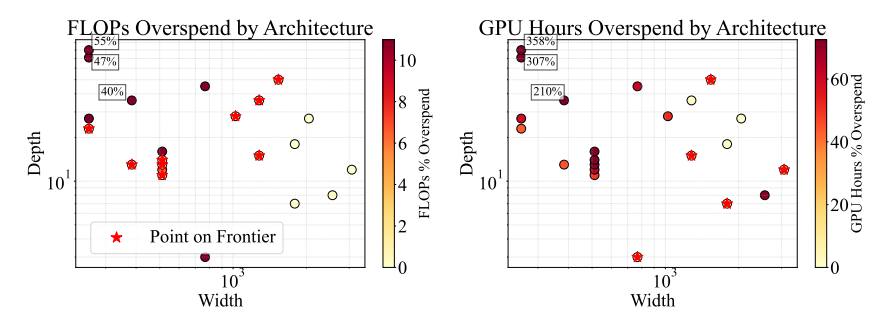


Figure 16: The inefficiency of training models with suboptimal widths and depths. We plot the FLOPs (left) and GPU Hours (right) *overspend* after training our Gemstones for 300 billion tokens. We define the overspend as how many resources (FLOPs or GPU hours) are required for a model with a given width-depth configuration to reach some target loss, relative to the models that achieve that target loss the fastest (the "points on (pareto)-frontier"). We can see that the skinny models (top-left, dark points) use many more FLOPs or GPU hours to reach a target loss than the wide models. We note that these inefficiencies exist in our training setup because we only use tensor parallelism and not pipeline parallelism but highlight how to easily transfer these results to other environments in Section 4.4.

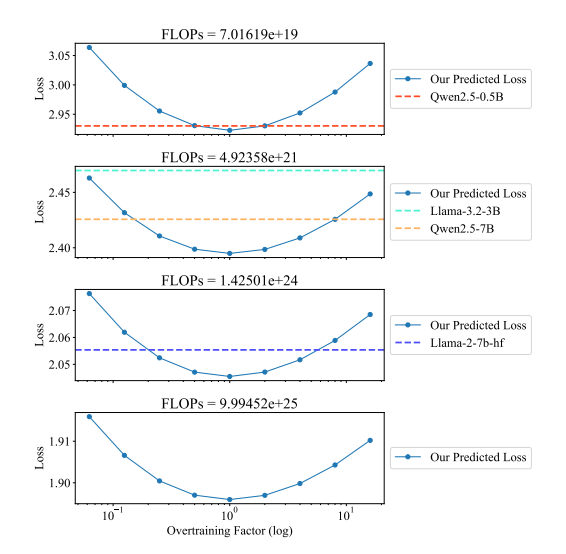


Figure 17: Quantifying the cost of overtraining. We simulate deviations from our prescriptions to assess their impact on model performance by increasing the optimal token count prescribed by an overtraining factor. We then optimize the model shape to achieve the lowest loss possible at each FLOP budget and overtraining factor. Note that 10^{0} , or $1\times$, is the prescribed optimal point. We take four FLOP budgets (title of each plot) and plot the loss as a function of overtraining factor and see that under or overtraining increases predicted loss but by only a small amount. We plot the losses of selected open source models on our validation set to help ground the y-axis ranges.

J Training

Despite our best efforts to sufficiently mix the training data, we still see slight jumps in the global training loss when the training switches between chunks of data, hence we use validation loss to fit all laws as this is smooth.

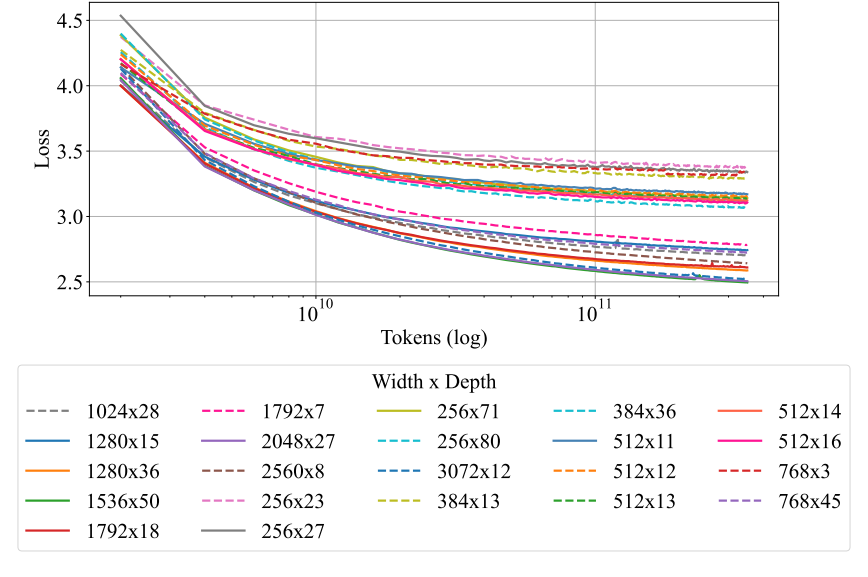


Figure 18: Loss curves for the main 22 training runs.

J.1 Loss Curves

J.2 Additional Training Complications

Any gemstone naturally contains a small number of inclusions or fractures. We discuss a few of the minor imperfections in our model collection below.

Dealing with Training Instabilities After some of the widest models were trained beyond 50B tokens we began to observe unrecoverable loss spikes that were proceeded by small wobbles in the loss trajectory. Under the general intuition that the culprit was most likely that the width/depth ratios considered were simply *too extreme* for existing initialization and learning rate scaling approaches to handle, we reran some of the models with a "patch" in place.

We modified the initialization rules and learning rate scaling factors to rescale the depth and layer indices of the model such that if width/depth > 256 scale variances and learning rates as if the depth of the model was actually $depth' = \lceil (width/100) \rceil$. The overall effect of the patch is to initialize and scale learning rates more conservatively, as if the aspect ratio were only 100 while keeping the original width of the model. We found this allowed us to complete training for a full set of 22 models out to 350B tokens for even our most extreme models.

However, after 350B tokens, despite these efforts we observed that most extreme models which were patched still diverged anyway. While a partial cause of this could be the constant learning rate scheduler employed during training, concurrent work, from the authors of the original OLMo paper and codebase [Groeneveld et al., 2024] from which we derived some of our choices, reported that the initialization scheme dubbed the "Mitchell-init" is indeed systematically prone to instabilities later on in training [OLMo et al., 2024]. While an unfortunate finding, we were unable to rerun all of our experiments due to the consumption of significant non-fungible compute resources in the original experiments.

Models Lacking Ablations Our cooldown ablation is from initial experiments below 100B tokens of training which do not use the patched learning rates scaling rules. This means there are minor discrepancies between the cooldown ablation and main set of training runs for the widest models from the three largest parameter count groups $(1792 \times 7, 2560 \times 8, 3072 \times 12)$. We also do not cool down the 100B token checkpoint for the 3072×12 model, as it was experiencing a loss spike at that final point. Finally, we do not include ablations for the two width 512 models which do not fall into the $\pm 5\%$ boundary of the 100M parameter count $(512 \times 11, 512 \times 14)$, as they were only added to the collection in later experiments.

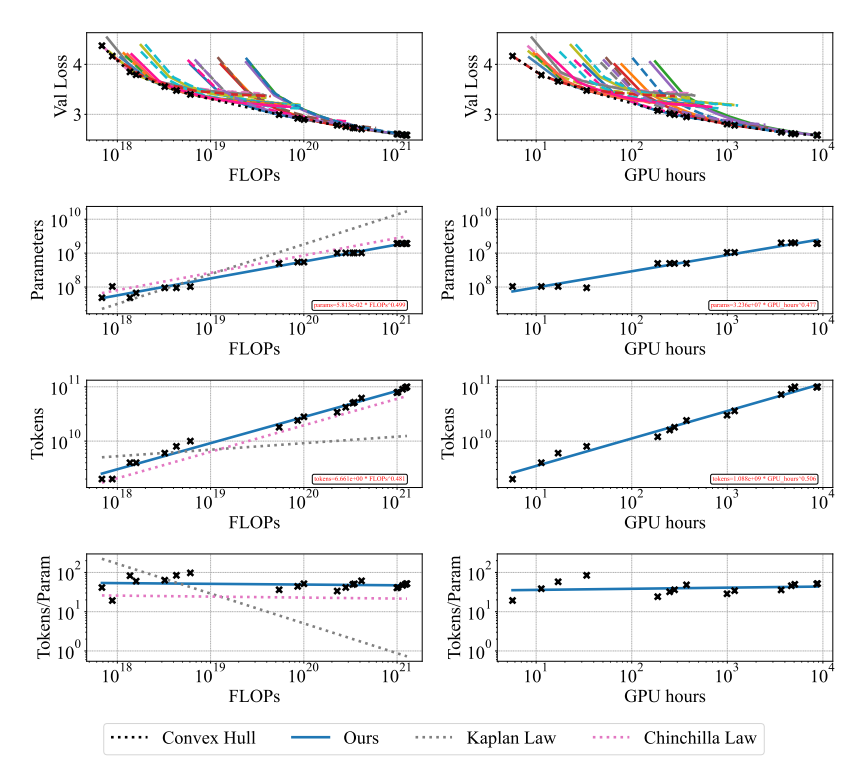


Figure 19: Extended Approach 1 plot from Figure 3, including tokens and parameters axes. As in Figure 3, we present an analysis over FLOPs on the left and over GPU hours take to train on the right.

K Ablations for Approach 1

K.1 Extended Paper Figures

In Figure 19, we plot an extended version of the Approach 1 plot we present in Figure 3.

K.2 Alternative Learning Rates

In Figure 20, we present the Approach 1 prescription when fitting on the learning rate ablation data.

K.3 Cooldown

In Figure 21, we present the Approach 1 prescription when fitting on the cooldown ablation data.

K.4 Varying Delta in the Huber loss

In Figure 22, where we plot the exponents found by optimizing the Huber loss versus the size of the grid search used for optimization. We see that a delta of 10^{-5} is unstable for smaller grid sizes and including more tokens in the fitting data generally increases stability of the exponents found during optimization.

L FLOP counting matters

In Figure 23 we show that the common approximation of FLOPs per token $6 \times parameters$, miscounts the true FLOPS by a significant amount.

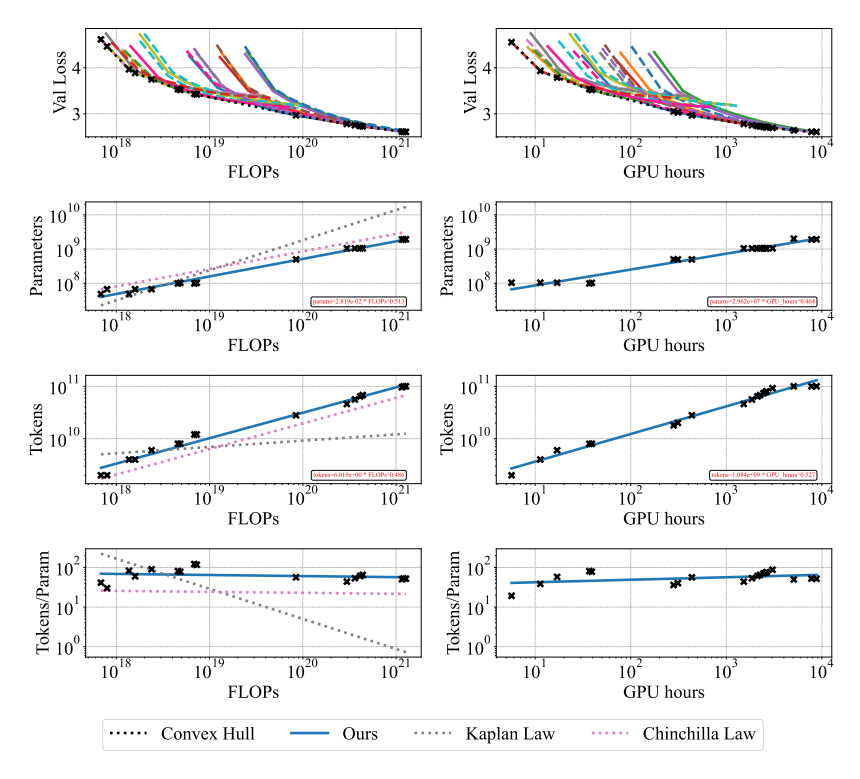


Figure 20: Approach 1 fitted on the learning rate ablation dataset. As in Figure 3, we present an analysis over FLOPs on the left and over GPU hours take to train on the right.

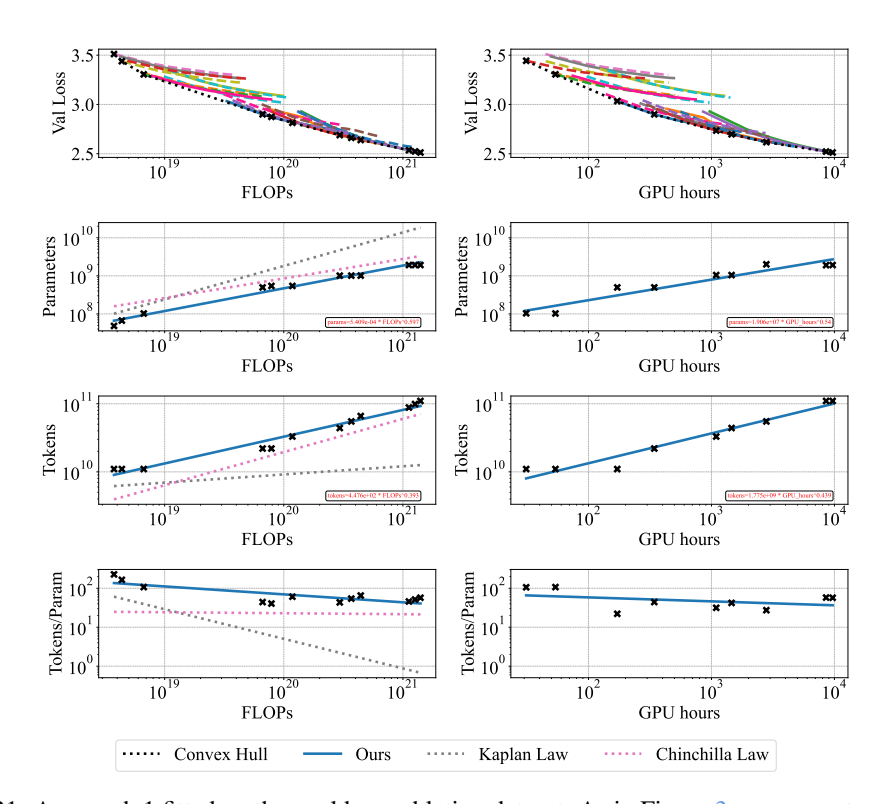


Figure 21: Approach 1 fitted on the cooldown ablation dataset. As in Figure 3, we present an analysis over FLOPs on the left and over GPU hours take to train on the right.

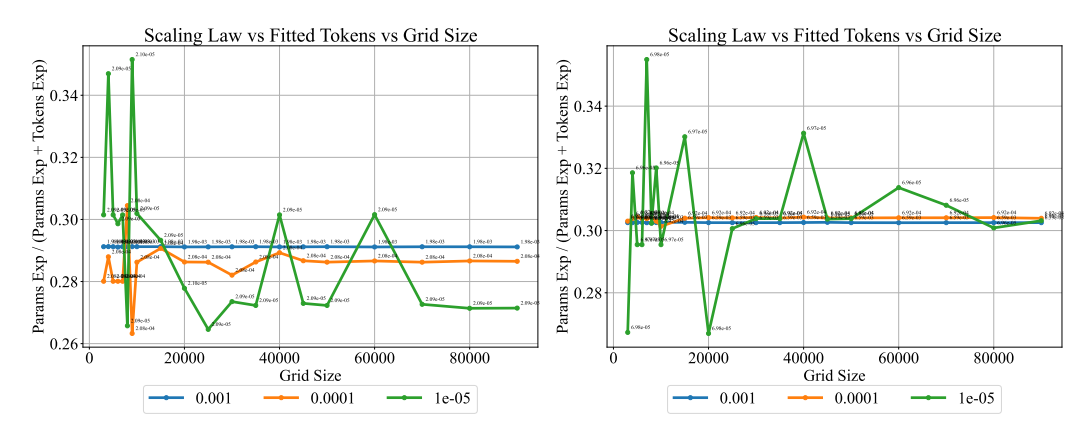


Figure 22: We plot the size of the grid search as the x axis and the gradient of the prescribed tokens as the y axis. We vary delta and see that a delta of 10^{-5} is highly unstable when fitting on smaller grid sizes. On the left, we plot only fitting on data less than 100 billion tokens. On the right, we plot fitting on all data up to 350 billion tokens. We see that including more data increases the stability of the exponents found for smaller grid sizes for deltas 10^{-4} , 10^{-5} .

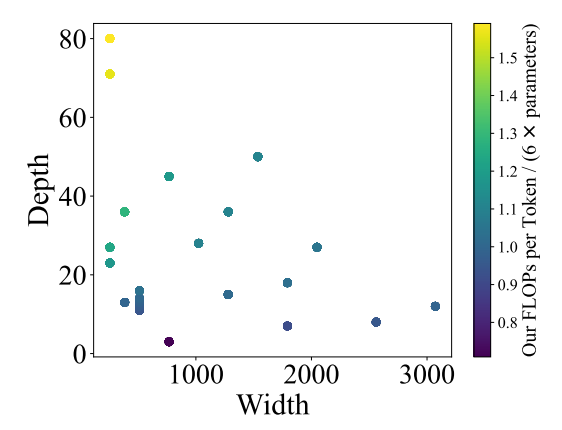


Figure 23: We color the points based on the ratio of our calculated FLOPs per token which is shown in the code below and using $6 \times parameters$. We see counting the FLOPs properly becomes more important for aspect ratios off outside of the standard regime.

```
VOCAB_OURS = 50304
SEQ_LEN = 2048
WORLD_BATCH_SIZE = 2048.0
HEAD_SIZE = 128
EXPAND_FACTOR = 4.0
def flops_per_token_gqa(
    width: NDArray[number]
                             number,
    depth: NDArray[number]
                             number,
    vocab_size=VOCAB_OURS,
    queries_per_group=2,
    seq_len=SEQ_LEN,
):
    Some details (negligible even for extremely wide models) omitted, including:
    * numerically stable softmax
    * softmax addition only being over rows
    * dot products being only n-1 additions (fused multiply-add exists anyway)
    num_qheads = width / HEAD_SIZE
```

```
num_kvheads = (
   2 * num_qheads / queries_per_group
embeddings = 0 # 0 if sparse lookup, backward FLOPs negligible
attention = 2.0 * seq_len * (num_qheads + num_kvheads) * width * HEAD_SIZE
attention += (
   3.5 * seq_len * (num_qheads + num_kvheads / 2) * HEAD_SIZE
) # RoPE, as implemented here/GPT-NeoX
# score FLOPs are halved because causal => triangular mask => usable sparsity
kq_logits = 1.0 * seq_len * seq_len * HEAD_SIZE * num_qheads
softmax = 3.0 * seq_len * seq_len * num_qheads
softmax_q_red = 2.0 * seq_len * seq_len * HEAD_SIZE * num_qheads
final_linear = 2.0 * seq_len * width * HEAD_SIZE * num_qheads
attn_bwd = (
   2.0 * attention
   + 2.5 * (kq_logits + softmax + softmax_q_red)
   + 2.0 * final_linear
) * depth
attention += kq_logits + softmax + softmax_q_red + final_linear
ffw_size = EXPAND_FACTOR * width
dense_block = (
   6.0 * seq_len * width * ffw_size
) # three matmuls instead of usual two because of GEGLU
dense_block += (
   10 * seq_len * ffw_size
) # 7 for other ops: 3 for cubic, two additions, two scalar mults
dense_block += 2.0 * width * seq_len # both/sandwich residual additions
rmsnorm = 2 * 7.0 * width * seq_len
final_rms_norm = 7.0 * width * seq_len # one last RMSNorm
final_logits = 2.0 * seq_len * width * vocab_size
nonattn_bwd = 2.0 * (
   embeddings + depth * (dense_block + rmsnorm) + final_rms_norm + final_logits
forward_pass = (
   embeddings
   + depth * (attention + dense_block + rmsnorm)
   + final_rms_norm
   + final_logits
backward_pass = attn_bwd + nonattn_bwd # flash attention
return (forward_pass + backward_pass) / seq_len
```